The Aeronautical Journal (2024), **128**, pp. 1071–1103
doi:10.1017/aer.2024.10

ROYAL AERONAUTICAL SOCIETY

RESEARCH ARTICLE

On the conditions for absolute minimum fuel burn for turbofan powered, civil transport aircraft and a simple model for wave drag

D.I.A. Poll[1] and U. Schumann[2]

Aerospace Engineering, Cranfield University, Cranfield, UK and Deutsches Zentrum für Luft- und Raumfahrt, Institut für Physik der Atmosphäre, Oberpaffenhofen, Germany
Corresponding author: D.I.A. Poll; Email: d.i.a.poll@cranfield.ac.uk

Received: 28 July 2023; **Revised:** 14 January 2024; **Accepted:** 17 January 2024

Keywords: turbofan aircraft performance; fuel flow rate; engine overall efficiency; optimum flight conditions; best flight conditions; wave drag

Abstract

In a recent series of papers, Poll and Schumann have been developing a simple model for estimating fuel burn for turbofan powered, civil transport aircraft for a given mass, Mach number and flight level and in a specified ambient temperature profile for all phases of flight. This paper focuses upon the combination of Mach number and flight level at which an aircraft cruises with the absolute minimum fuel burn. For a given aircraft type, the information necessary to determine these conditions must be specified and this poses a challenge. An initial attempt to obtain these data has been described previously by the first author. In this paper, the optimum conditions are found using a completely different approach. Starting from first principles and using established theory, the equations governing the situation where engine overall efficiency and airframe lift-to-drag ratio both have local maxima at the same flight condition are developed. This special case is termed the "design optimum" condition and, for a specified aircraft mass and a specified atmospheric temperature versus pressure profile, it gives the lowest possible fuel burn for any aircraft and engine combination. The design optimum occurs at a particular Mach number and Reynolds number, and it is a fixed characteristic of the aircraft. The analysis reveals the significance of Reynolds number variations, wave drag, including its derivatives with respect to both lift coefficient and Mach number, and the atmospheric properties. Whilst wave drag is notoriously difficult to determine accurately, it is found that solutions to the equations are not particularly sensitive to the accuracy of this quantity. Consequently, a simple, physically realistic model can give good results. An appropriate model is developed and a complete, approximate solution is obtained. Taking the International Standard Atmosphere as the design atmosphere, results are presented for the 53 aircraft types previously considered by Poll and Schumann. Relative to the design optimum conditions, when Reynolds number is constant and wave drag is zero, compressibility alone reduces L/D by about 5%, reduces lift coefficient by about 1.5% and increases drag coefficient by about 3.5%. Reynolds number variation has little effect upon L/D, but it reduces lift coefficient and drag coefficient by a further 7% and 8% respectively. The reduction in lift coefficient has a significant impact on the optimum cruise flight level.

In general, an aircraft's operating optimum will not coincide with its design optimum, but deviations are expected to be small. Therefore, using the design optimum solution as a reference point, an improved version of the operating optimum estimation method described by Poll and Schumann in previous work is developed. This allows the estimation of the conditions for absolute minimum fuel burn for an aircraft of given mass flying thorough any atmosphere. Updated coefficients for the 53 aircraft types are given.

Nomenclature

AR	wing aspect ratio
a	constant in the skin friction law – Equation (17)
a_∞	speed of sound $= (\gamma \Re T_\infty)^{1/2}$

© The Author(s), 2024. Published by Cambridge University Press on behalf of Royal Aeronautical Society. This is an Open Access article, distributed under the terms of the Creative Commons Attribution licence (http://creativecommons.org/licenses/by/4.0/), which permits unrestricted re-use, distribution and reproduction, provided the original article is properly cited.
https://doi.org/10.1017/aer.2024.10 Published online by Cambridge University Press

BPR	engine nominal bypass ratio
b	constant in the skin friction law – Equation (17)
b_f	maximum fuselage width
Cd	airframe drag coefficient $= D/(q_\infty S_{ref})$
Cd_o	zero-lift drag coefficient
Cd_w	wave drag coefficient
C_L	overall lift coefficient $= L/(q_\infty S_{ref})$
C_F	mean skin friction coefficient – Equation (17)
C_T	aircraft total net thrust coefficient $= F_n/(q_\infty S_{ref})$
D	total drag force
e	aircraft Oswald efficiency factor – Equation (20)
FL	flight level
F_n	net installed thrust, summed over all engines
g	acceleration due to gravity (9.80665 m/sec^2 at sea level)
j_1, j_2, j_3	constants in the wave drag model – Equations (38) and (79)
K	lift dependent drag factor – Equation (18)
k_1	miscellaneous lift-dependent drag factor – Equation (22)
L	lift force
LCV	lower calorific value of fuel ($\approx 43 \times 10^6$ J/kg for kerosene)
L/D	lift-to-drag ratio
l	characteristic streamwise length $= S_{ref}^{1/2}$
M_∞	flight Mach number $= V_\infty / a_\infty$
M_{crit}	critical Mach number
M_{cc}	crest critical Mach number
M_{DD}	drag divergence Mach number
M_{TF}	aerofoil technology level factor – Equation (34)
$MTOM$	maximum permitted take-off mass
m	instantaneous total aircraft mass
m_f	instantaneous fuel mass
p	static pressure
q_∞	freestream dynamic pressure $= 0.5\rho_\infty (V_\infty)^2 = 0.5\gamma p_\infty (M_\infty)^2$
R^{ac}	characteristic Reynolds number – Equation (4)
$\Re$	gas constant for air (287.05 J/(kg K))
S	distance travelled through the air
S_{ref}	aerodynamic reference wing area (Airbus definition)
s	wingspan
T	static temperature
t/c	wing thickness-to-chord ratio in the streamwise direction
V_∞	true air speed
X	wave drag variable – Equation (31)
γ	ratio of specific heats for air (=1.4)
δ	wave drag parameter – Equation (41)
δ_1	wing vortex drag factor – Equation (20)
δ_2	vortex drag wing-fuselage interference factor – Equation (20)
η_o	propulsion system overall efficiency – Equation (1)
η_1, η_2	constants in Equation (11)
ι	atmospheric constant – Equation (A-7)
κ	atmospheric constant – Equation (64)
Λ_w	wing quarter-chord sweep angle
μ	dynamic viscosity
ϕ	atmospheric parameter – Equation (A-5)
ρ	air density $= p/(\Re T)$
τ	constant coefficient – Equations (59) and (C-4)
$\psi_{0\text{-}7}$	aircraft characteristic coefficients – Equations (16), (67), (60), (66), (54), (56), (58) and (62)
ω	atmospheric constant – Equation (A-5)

https://doi.org/10.1017/aer.2024.10 Published online by Cambridge University Press

Superscripts

ac	whole aircraft value
M	at constant Mach number
P	at constant pressure or constant flight level
R	at constant Reynolds number

Subscripts

avg	average value
B	best, or local maximum, value
DO	design optimum condition
ISA	in the International Standard Atmosphere
LS	low speed
LRC	long-range cruise
max	maximum value
MRC	maximum-range cruise
min	minimum value
OO	operational optimum condition
TP	at the tropopause
∞	flight, or freestream, value

1.0 Introduction

Accurate models for the performance of civil jet transport aircraft are important elements in the determination of aviation's impact upon the environment. The environmental science community needs estimation methods not only for the levels of the various emissions in jet engine exhaust, but also the altitude at which they are released and, in the case of contrail formation, the overall efficiency of the engine. This information is needed for older aircraft so that historic databases can be analysed with greater accuracy and also for new and projected aircraft so that future environmental impact may be assessed.

Currently, the community relies heavily on "black box" methods such as BADA [1] and PIANO [2]. However, neither method is "open source", they have not been subjected to independent peer review, nor has their output been fully validated in the open literature. In addition, whilst there is a free version of PIANO, known as PIANO-X, the full version is a commercial product and, without payment for a full licence, the differences between PIANO-X and PIANO are not visible. BADA is administered by EUROCONTROL. It is not freely available to the general academic community and both its use and the publication of results is controlled via a restrictive, licencing agreement. Importantly, it is not known whether either of these methods produce accurate results in a general atmosphere, or whether, as the needs of environmental science become more detailed and more precise, these methods are becoming a weak link in an important chain. Consequently, there is a need for aircraft performance methods that are open source, fully transparent, developable, capable of independent validation and freely available to all.

In a recent series of papers, Poll [3] and Poll and Schumann [4, 5] have constructed a simple method model for fuel burn estimation of civil transport aircraft. This provides a fully transparent, public domain alternative to the BADA and PIANO codes. Application of the method requires a knowledge of the Mach number and flight level at which an aircraft with a specified mass, flying in a specified atmosphere has its absolute minimum fuel burn rate. However, this information is not easy to obtain, and an initial attempt is described in Poll and Schumann [5] where input files are provided for 53 aircraft types.

This paper re-examines the problem of determining absolute minimum fuel burn using a first principles approach based upon established theory. The equations governing the optimum conditions in a general atmosphere are derived and a complete, though approximate, solution is obtained using a simple

https://doi.org/10.1017/aer.2024.10 Published online by Cambridge University Press

wave drag model. This solution not only gives a full physical picture of the conditions at the optimum, but it can also be used to improve the accuracy of the input files for the Poll and Schumann [4, 5] method.

2.0 Background

If the overall propulsive efficiency of the engine, η_o, is defined as

$$\eta_o = \frac{F_n V_\infty}{\dot{m}_f LCV}, \tag{1}$$

where F_n is the total net, installed[1] thrust, V_∞ is the true airspeed, $\dot{m}_f$ is the fuel mass flow per unit time and LCV is the lower calorific value of the fuel, then the fuel consumption per unit distance travelled through the air is

$$\frac{dm_f}{dS} = \frac{\dot{m}_f}{V_\infty} = -\frac{dm}{dS} = \left(\frac{F_n}{D}\right)\left(\frac{L}{(\eta_o L/D)\, LCV}\right). \tag{2}$$

Here m is the instantaneous total mass of the aircraft, S is the distance travelled through the air, L is the lift and D is the drag.

In the steady state cruise, lift is equal to weight and thrust is equal to drag[2]. Hence,

$$\frac{dm_f}{dS} = \left(\frac{mg}{(\eta_o L/D)\, LCV}\right), \tag{3}$$

where g is the acceleration due to gravity. Therefore, the rate at which fuel is consumed in cruise is governed by the single aero-thermodynamic parameter $(\eta_o L/D)$. Dimensional analysis reveals that, in general, this quantity is a function of the flight Mach number, M_∞ and the flight Reynolds number, R^{ac}. Following Poll and Schumann [4], Reynolds number is defined as

$$R^{ac} = \frac{l\rho_\infty V_\infty}{\mu_\infty} = S_{ref}^{1/2}\left(\frac{\rho_\infty a_\infty}{\mu_\infty}\right) M_\infty = S_{ref}^{1/2}\left(\frac{\gamma p_\infty}{\mu_\infty a_\infty}\right) M_\infty, \tag{4}$$

whilst the aircraft lift, drag and thrust coefficients have their usual definitions, i.e.

$$C_L = \frac{L}{q_\infty S_{ref}},\ C_D = \frac{D}{q_\infty S_{ref}} \text{ and } C_T = \frac{F_n}{q_\infty S_{ref}} \text{ where } q_\infty = \frac{\gamma}{2} p_\infty M_\infty^2. \tag{5}$$

Here, air is taken to be an ideal gas, l is a "typical" aircraft reference length, taken to be the square root of the reference wing area, S_{ref}, p_∞ is the atmospheric static pressure, ρ_∞ the density, a_∞ the local speed of sound, μ_∞ the dynamic viscosity and γ is the ratio of specific heats.

In practise, aircraft do not cruise at a fixed altitude. Rather, to maintain safe separation in the vertical direction, they follow isobars, i.e. they fly in such a way that the local static pressure, p_∞, is held constant. By international agreement, values of static pressure are converted into "flight levels", which are the altitudes, measured in feet, that the aircraft would have if it was operating in the International Standard Atmosphere (*ISA*) [6] divided by 100 feet.

3.0 Conditions for optimum ($\eta_o L/D$) and the design optimum

In Poll [3] it was shown that, for an aircraft with a specified mass and Mach number in steady, straight and level flight, there is a lift coefficient, $(C_L)_B$, at which $(\eta_o L/D)$ has a local maximum, or best, value. Furthermore, there is a particular combination of Mach number, M_o, and lift coefficient, $(C_L)_o$, at which

[1] An engine installed in an aircraft delivers about 97% of the thrust of the same engine in isolation.

[2] In general, the engine thrust line will not be parallel to the flight direction and thrust will have components in both the lift and drag directions. However, for a civil transport aircraft the differences are very small and may be neglected without significant loss of accuracy.

https://doi.org/10.1017/aer.2024.10 Published online by Cambridge University Press

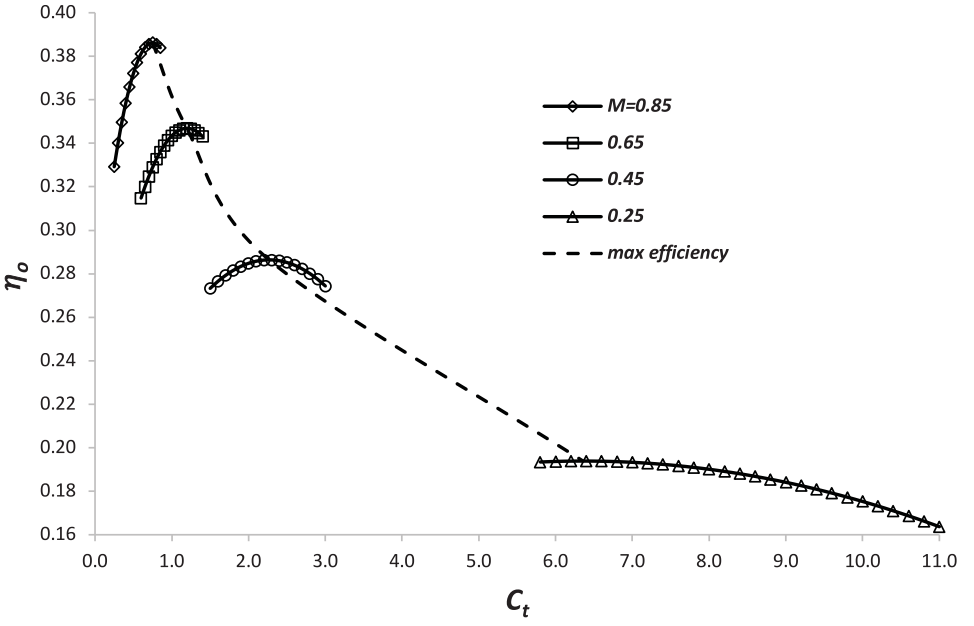

Figure 1. *The variation of overall efficiency with thrust coefficient and Mach number for a civil aircraft turbofan engine with a nominal bypass ratio of 8. Data taken from Jenkinson et al. [7].*

($\eta_o L/D$) has an absolute maximum, or optimum, value, i.e. the fuel burn per unit distance travelled through the air has an absolute minimum.

The conditions for optimum ($\eta_o L/D$) are determined by a balance between the gradients of η_o and L/D with respect to both Mach number, M_∞, and either flight level, or p_∞, i.e. when

$$d(\eta_o L/D) = \frac{\partial(\eta_o L/D)}{\partial M_\infty} dM_\infty + \frac{\partial(\eta_o L/D)}{\partial p_\infty} dp_\infty = 0. \tag{6}$$

In straight and level flight, thrust is equal to drag and, from the definition of lift coefficient,

$$\frac{M_\infty}{C_L}\left(\frac{\partial C_L}{\partial M_\infty}\right)^p = -2 \text{ and } \frac{p_\infty}{C_L}\left(\frac{\partial C_L}{\partial p_\infty}\right)^M = -1. \tag{7}$$

Therefore, Equation (6) is satisfied when

$$\frac{M_\infty}{\eta_o}\frac{\partial \eta_o}{\partial M_\infty} - \frac{M_\infty}{Cd}\frac{\partial Cd}{\partial M_\infty} - 2 = 0 \tag{8}$$

and

$$\frac{C_L}{Cd}\frac{\partial Cd}{\partial C_L}\left(1 - \frac{C_T}{\eta_o}\frac{\partial \eta_o}{\partial C_T}\right) - 1 = 0. \tag{9}$$

As discussed in Poll and Schumann [5] and as shown in Fig. 1, at fixed M_∞, engine overall efficiency, η_o, has a local maximum value at a particular value of the thrust coefficient, C_T. This maximum is strongly dependent upon the Mach number and, provided that M_∞ is greater than 0.2[3] may be represented by a power law, i.e. when

[3]Equation (11) gives the correct value of $(\eta_o)_B$ when M_∞ is zero. However, with the exception of the special case when η_2 is unity, the gradient of $(\eta_o)_B$ with respect to M_∞ when M_∞ is zero is infinite and this cannot be correct. To avoid this problem, Equation (11) should only be used when M_∞ is greater than about 0.2.

https://doi.org/10.1017/aer.2024.10 Published online by Cambridge University Press

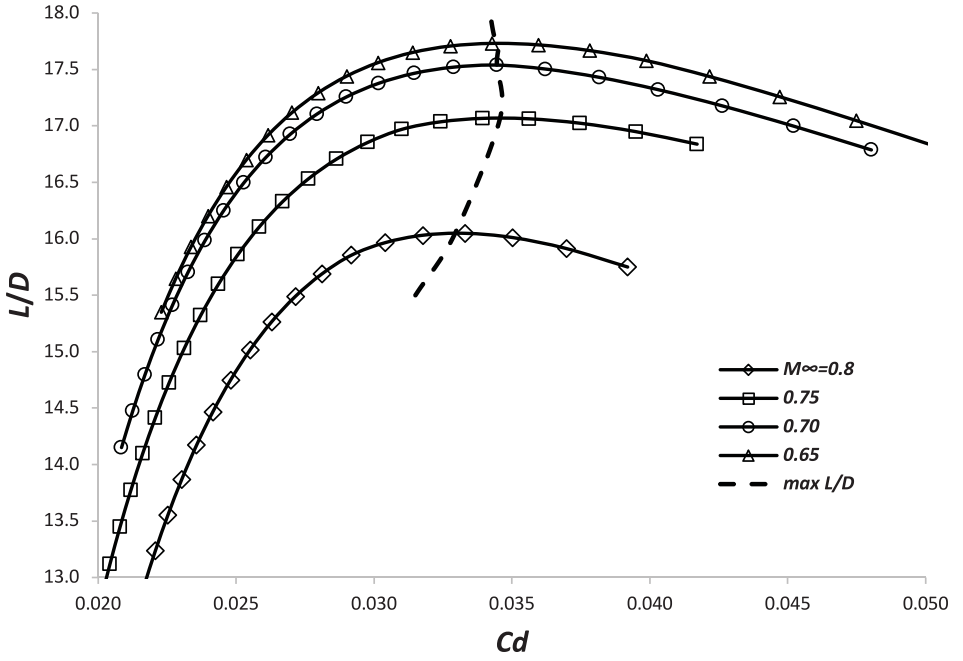

Figure 2. *An example of the variation of aircraft lift-to-drag ratio with drag coefficient and Mach number when the mass is fixed.*

$$\frac{C_T}{\eta_o}\frac{\partial \eta_o}{\partial C_T} = 0, \tag{10}$$

$$(\eta_o)_B \approx \eta_1 (M_\infty)^{\eta_2}, \tag{11}$$

where the coefficients η_1 and η_2 are constant and depend upon the engine type. It follows that

$$\left(\frac{M_\infty}{\eta_o}\frac{\partial \eta_o}{\partial M_\infty}\right)_B = \eta_2. \tag{12}$$

Similarly, as shown in Fig. 2, when the mass and Mach number are fixed, the aircraft lift-to-drag ratio has a local maximum at a particular value of the drag coefficient. However, in this case, the maximum L/D reduces as Mach number increases.

In order to have the absolute maximum value of ($\eta_o L/D$) the airframe and engine must be "perfectly" matched, i.e. both η_o and L/D must have local maxima at the same values of Mach number and drag (= thrust) coefficient. However, this can only be achieved at a single condition. Hence, for specified mass and a specified atmosphere, there is only one possible combination of Mach number and Reynolds number. Since this condition is fixed in the design process, it is appropriate to call it the "design optimum" condition and the corresponding flight condition is a characteristic of the airframe-engine combination. Hence, at the design optimum, Equations (8) and (9) become

$$\left(\frac{M_\infty}{Cd}\frac{\partial Cd}{\partial M_\infty}\right)_{DO} = \eta_2 - 2 \tag{13}$$

and

$$\left(\frac{C_L}{Cd}\frac{\partial Cd}{\partial C_L}\right)_{DO} = 1. \tag{14}$$

https://doi.org/10.1017/aer.2024.10 Published online by Cambridge University Press

These are completely general relations that define the design optimum value of $(\eta_o L/D)$ in any specified design atmosphere and the conditions at which it occurs.

4.0 Estimation of the drag

If Equations (13) and (14) are to be solved, it is necessary to know the relation linking the drag coefficient to the lift coefficient and Mach number, otherwise known as the aircraft's "drag polar". For Mach numbers greater than 0.5, the cruise drag coefficient may be expressed in the form proposed by Shevell [8], i.e.

$$Cd \approx Cd_0 + KC_L^2 + Cd_w. \tag{15}$$

The first term, Cd_o, is the zero-lift drag coefficient and the standard approximation is that this is directly proportional to the aircraft's mean skin-friction coefficient, C_F^{ac}. Hence,

$$Cd_0 = \psi_0 C_F^{ac}, \tag{16}$$

where ψ_0 depends upon the aircraft geometry. In general, Cd_0 also depends upon M_∞. This is because increasing the Mach number increases surface temperature[4] and modifies the surface pressure distribution. The result is that skin friction reduces and the pressure, or 'form', drag increases, i.e. the constant of proportionality linking Cd_0 and (C_F^{ac}) increases. However, for Mach numbers above 0.5, the net effect is a cancellation making Cd_0 approximately independent of Mach number, see Shevell [8] (Chapter 12). Poll and Schumann [4] have shown that the relationship between skin friction and Reynolds number, at a Mach number of 0.5, can be approximated by the power law

$$C_F^{ac} \approx \frac{a}{(R^{ac})^b}, \tag{17}$$

where a and b are constants having values of 0.0269 and 0.14, respectively.
The second term, K, is known as the low-speed, lift-dependent drag factor, and is given by

$$K = \frac{1}{\pi .AR.e_{LS}}. \tag{18}$$

Here, AR is the wing aspect ratio, defined as

$$AR = \frac{s^2}{S_{ref}}, \tag{19}$$

where s is the wingspan and e_{LS} is the low-speed Oswald efficiency factor.

The Oswald factor captures all the lift-dependent drag effects of which vortex drag on the wings is the primary source. However, the tailplane and the fuselage also generate vortex drag. In addition, there are non-vortex, lift-dependent drag contributions arising because a change in lift alters the pressure distribution over the various components, which, in turn, alters their profile drag. Therefore, the Oswald factor is complex and, as explained by Shevell [8], it is primarily a function of aircraft geometry and Cd_o and is given, approximately, by

$$e_{LS} \approx \frac{1}{\delta_1 + \delta_2 + \pi .AR.k_1}. \tag{20}$$

Again following Shevell, δ_1 is a constant representing the wing vortex drag and is typically about 1.03, whilst δ_2 represents the interference effect between the wing and the fuselage, which may be approximated by

$$\delta_2 \approx 2\left(\frac{b_f}{s}\right)^2, \tag{21}$$

[4]The usual assumption is that there is no heat transfer taking place at the surface, i.e. the surface is adiabatic.

https://doi.org/10.1017/aer.2024.10 Published online by Cambridge University Press

with b_f being the fuselage maximum width and k_1 is the non-vortex, lift-dependent drag factor, where, as discussed in Poll and Schumann [5],

$$k_1 \approx 0.80(1 - 0.53\, cos(\Lambda_w))Cd_0, \tag{22}$$

where Λ_w is the wing quarter-chord sweep angle. Hence,

$$K = \frac{1}{\pi .AR.e_{LS}} \approx k_1 + \left(\frac{1.03 + \delta_2}{\pi .AR}\right). \tag{23}$$

Finally, the third term, Cd_w, is the "wave drag" coefficient. For an aerofoil at a given angle-of-attack, as the flight speed increases from a low starting value, sonic conditions will eventually be reached at the point on the surface where the local static pressure is lowest. Usually, this point is close to the leading edge on the wing's upper surface and the corresponding flight Mach number is called the "critical" value, M_{crit}. Further increases in speed result in the formation of a region of supersonic flow that is bounded by the wing surface, a "sonic interface"[5] and, if the Mach number is sufficiently high, a terminating shockwave. Once a "supersonic zone" is established, increases in either M_∞, or C_L, produce an increase in drag and the terminating shockwave moves rearwards. When this zone is confined to the front portion of the wing, the drag increases are modest, being typically less than 10 drag counts[6] – see, for example, Torenbeek [9] (Section 4.6). Consequently, the variation is known as "drag creep". However, when the terminating shockwave moves onto the rear part of the wing, the rate of drag rise with increasing Mach number, or increasing C_L, becomes large and this is usually referred to as "drag rise". Since both the creep and rise regimes are linked to the formation and subsequent development of shockwaves, the resulting drag increments are collectively referred to as "wave" drag.

In the current approach, since, by definition, both Cd_0 and K are independent of Mach number, Cd_w captures all the additional effects due to compressibility and, once this is specified as a function of Mach number and lift coefficient, the drag polar is complete.

As shown in detail in Appendix A, the conditions at the design optimum condition are obtained by differentiating the drag polar and, after some manipulation, it is found that, to a very good approximation, in a completely general atmosphere, the design optimum values for C_L, Cd and L/D are given by

$$(C_L)_{DO} \approx \left(1 - \frac{1}{2}\left(b\left(1 + \left(\frac{k_1}{K}\right)\right)(1 + \Gamma_{DO}) + \left(\frac{Cd_w}{Cd_0}\right)_{DO}\left(\left(\frac{C_L}{Cd}\frac{\partial Cd_w}{\partial C_L}\right)_{DO} - 1\right)\right)\right)\left(\frac{Cd_0}{K}\right)^{1/2}_{DO} \tag{24}$$

and, using equation (15),

$$(Cd)_{DO} \approx 2\left(1 - \frac{1}{2}\left(b\left(1 + \left(\frac{k_1}{K}\right)\right)(1 + \Gamma_{DO}) + \left(\frac{Cd_w}{Cd_0}\right)_{DO}\left(\left(\frac{C_L}{Cd_w}\frac{\partial Cd_w}{\partial C_L}\right)_{DO} - 2\right)\right)\right)(Cd_0)_{DO}. \tag{25}$$

Hence,

$$\left(\frac{L}{D}\right)_{DO} \approx \frac{1}{2}\left(1 - \frac{1}{2}\left(\frac{Cd_w}{Cd_0}\right)_{DO}\right)\left(\frac{1}{KCd_0}\right)^{1/2}_{DO}. \tag{26}$$

Provided that Equation (15) is used as the definition for Cd_w, these relations show how the wave drag, the Reynolds number and the atmospheric parameters affect the values of C_L, Cd and L/D when $(\eta_o L/D)$ is at its design optimum value.

[5]The surface formed by all the points in the flow field where the local Mach number is unity.

[6]1 drag count is equal to a change of 0.0001 in Cd.

https://doi.org/10.1017/aer.2024.10 Published online by Cambridge University Press

5.0 Representation of the wave drag

Wave drag is a very complex phenomenon, but, under normal cruising conditions, it accounts for only about 3% of the total, see Torenbeek [9] (Fig. 14.6). Nevertheless, its strong dependence upon Mach number and lift coefficient means that it has an influence on the aircraft's maximum lift-to-drag ratio and the flight conditions at which this occurs. Accurate, simple models of wave drag are rare. However, there is one method that captures enough of the underlying physics to provide a reasonably accurate, qualitative and quantitative description of the process.

Based on the experimentally determined drag characteristics of early, two-dimensional, transonic aerofoil sections, Shevell [8], but see also Shevell and Bayan [10] and Shevell [11], suggested that, whilst "drag creep" develops when M_∞ exceeds M_{crit}, the onset of "drag rise" is linked to the establishment of sonic conditions at the aerofoil "crest". This is the point on the aerofoil's upper surface that is parallel to the free-stream direction and locally sonic conditions are established there when M_∞ reaches the "crest critical" Mach number, M_{cc}. Shevell observed that M_{cc} depends, primarily, upon wing geometry and the lift coefficient, whilst the wave drag coefficient itself is governed by the ratio of M_∞ to M_{cc}.

Shevell proposed a method for estimating M_{cc} from a knowledge of the mean thickness-to-chord ratio and $C_{L.}$ Unfortunately, it is both complex and implicit. However, as can be seen in Ref. [8] (Fig. 12.7), for the ranges of thickness-to-chord ratio, t/c, and lift coefficient of practical interest, M_{cc} may be adequately represented by the relation

$$(M_{CC})_{2-D} \approx 0.88 - 0.18(C_L)_{2-D} - 0.92\,(t/c)\,. \tag{27}$$

This result applies to aerofoils with "peaky" pressure distributions, i.e. those having a very low pressure in a narrow region on the upper surface very close to the leading edge, that were typical of the high-speed aerofoil designs developed in the 1960s and 1970s.

An important application of Shevell's method is the determination of the aerofoil's drag "divergence" Mach number, M_{DD}. This is the value above which the drag is deemed, somewhat arbitrarily, to increase very rapidly with increasing flight Mach number. For historical reasons, there are two definitions for M_{DD} in general use. The first, introduced by the Douglas Aircraft Company, is the Mach number at which, for a fixed lift coefficient, the gradient $\partial Cd/\partial M_\infty$ reaches a specified value. Depending on the aerofoil, this may be either 0.05 or 0.1. The second is the Mach number that gives a fixed drag increase relative to the incompressible value for the same lift coefficient, i.e. a specific increment in Cd_w. According to Raymer, [12] the Boeing Company has used this definition, with the drag increment taken to be 20 counts. Clearly, when the Mach number is close to M_{DD}, the drag coefficient will be rising rapidly and these three criteria will yield similar results, with Shevell's relations suggesting that

$$\left(\frac{(M_{DD})_{20}}{M_{CC}}\right)_{2-D} \approx 1.03,\ \left(\frac{(M_{DD})_{0.05}}{M_{CC}}\right)_{2-D} \approx 1.02 \text{ and } \left(\frac{(M_{DD})_{0.1}}{M_{CC}}\right)_{2-D} \approx 1.045. \tag{28}$$

The significant point of note is that M_{DD} and M_{cc} are related by a simple factor that is close to unity. This implies that the qualitative physical argument for M_{cc} and Shevell's complex, first principles, estimation method is neither necessary, nor does it even need to be valid, since M_{cc} can just be viewed as a simple reference Mach number for the onset of drag rise. Hence, if the divergence Mach number is known for a given aerofoil section, it can be used to estimate the corresponding value of M_{cc}. This is fortuitous, since M_{DD} has received more attention in the open literature than M_{cc}. Consequently, the modified "Shevell method" may be applied to any aerofoil whose divergence Mach number is known.

The "peaky" aerofoil sections used in the original analysis were superseded by the much improved "supercritical" designs with higher intrinsic values of M_{DD} and reduced sensitivity to changes in C_L. The general behaviour of more modern aerofoils is given by the well-known "Korn" equation, which appears in many references, e.g. Torenbeek [9], Mason [13] and Boppe [14] and is

$$((M_{DD})_{0.1})_{2-D} \approx M_{TF} - 0.10(C_L)_{2-D} - 1.00\,(t/c)\,, \tag{29}$$

https://doi.org/10.1017/aer.2024.10 Published online by Cambridge University Press

where M_{TF} is a constant "aerofoil technology" factor. Shevell [8] suggests that, for supercritical aerofoils, M_{TF} falls in the range of 0.93 to 0.97, which is consistent with the average value of 0.95 quoted by Mason [13].

Whilst the arguments behind the method are based upon 2-D aerofoil characteristics, the governing relations may be extended to cover swept wings of infinite span by applying the standard "infinite sheared wing" transformation. This means that streamwise aerofoil section geometry is held constant as the sweep angle, Λ_w, is increased, whilst allowing no variation of any geometric characteristic, or flow property, in the direction parallel to the leading edge. Using the results from Equations (28) and (29), the extended model becomes

$$M_{CC} \approx 0.91 - 0.10\left(\frac{C_L}{cos^2(\Lambda_w)}\right) - 0.96\left(\frac{t/c}{cos(\Lambda_w)}\right) \tag{30}$$

and

$$X = \frac{M_\infty cos(\Lambda_w)}{M_{CC}}, \tag{31}$$

where

$$Cd_w \approx cos^3(\Lambda_w)\, function(X)\,. \tag{32}$$

These expressions are exact for an isolated, infinite-swept wing, but, on a full aircraft configuration, wave drag could also develop on the fuselage and other surfaces. However, as noted by Shevell [8] on a "well-designed" aircraft, the wave drag will always be dominated by the contribution from the wing and it will be assumed that all the aircraft to be considered in this study are "well designed".

On an aircraft wing, the span is finite and, in general, the local lift, streamwise chord, aerofoil section and twist will all vary in the spanwise direction. In addition, the fuselage influences the wing flow by modifying both the spanwise lift distribution and the local freestream velocity. All these effects influence wave drag development. Nevertheless, since most of the wave drag will be generated by the wing, by using the aircraft's total lift coefficient, an "average" value for t/c and taking Λ_w to be measured at the mean $^1/_4$ chord line, Equations (30), (31) and (32) can still provide the basis for a reasonable approximation of the wave drag for a complete aircraft configuration.

High Mach number drag data for total aircraft configurations rarely appear in the open literature. However, Obert [15] (Chapter 24) gives some useable information on the variation of drag coefficient with Mach number at various, fixed values of lift coefficient for thirteen civil transport aircraft. It is not always clear where these data have come from, or how accurate they are, and all are presented in very small figures. Nevertheless, divergence Mach number data for the aircraft's "average" aerofoil section have been extracted by assuming that pressure related drag acts in the direction normal to the $^1/_4$ chord line and applying the "20 additional drag counts" definition in that plane. The results are given in Fig. 3.

In every case, M_{DD} decreases as the total aircraft C_L increases and, using a straight line fit, slope and intercept values were obtained for each case. Averaging these gives

$$M_{DD} \approx 0.76 - 0.11\left(\frac{C_L}{cos^2(\Lambda_w)}\right) \tag{33}$$

and, using equation (28), it follows that, for the full aircraft configuration,

$$(M_{cc})^{ac} = (M_{TF})^{ac} - 0.10\left(\frac{C_L}{cos^2(\Lambda_w)}\right) \approx 0.74 - 0.10\left(\frac{C_L}{cos^2(\Lambda_w)}\right). \tag{34}$$

where $(M_{TF})^{ac}$ is a constant that captures the aerofoil technology factor plus the effect of the wing thickness-to-chord ratio and, consequently, is a characteristic of the aircraft. As indicated in Fig. 3, the average factor of 0.74 is subject to an uncertainty of at least ±7%. However, most importantly, the data suggest that the gradient dM_{CC}/dC_L for the full aircraft configuration is close to that for the wing in isolation.

Finally, Shevell [8] (Fig. 12.13) gives a single, empirical curve for the approximate variation of total aircraft Cd_w with the parameter X and this is given in Fig. 4.

https://doi.org/10.1017/aer.2024.10 Published online by Cambridge University Press

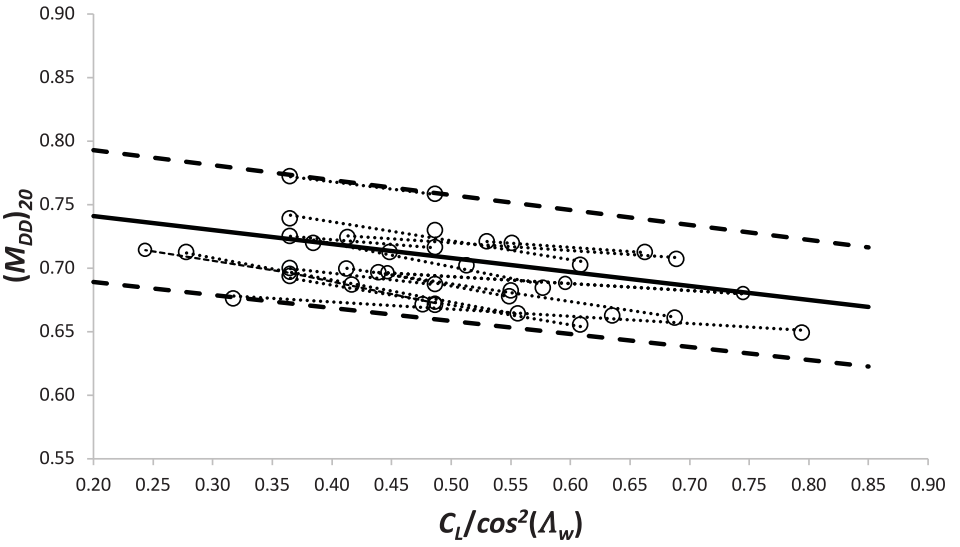

Figure 3. *The approximate variation of mean aerofoil, drag divergence Mach number with aircraft total lift coefficient for a range of aircraft types. Data are taken from Obert [15]. The solid line is Equation (33), the heavy dashed lines indicate ± 7% deviation and the light dashed lines show the trend for each individual aircraft.*

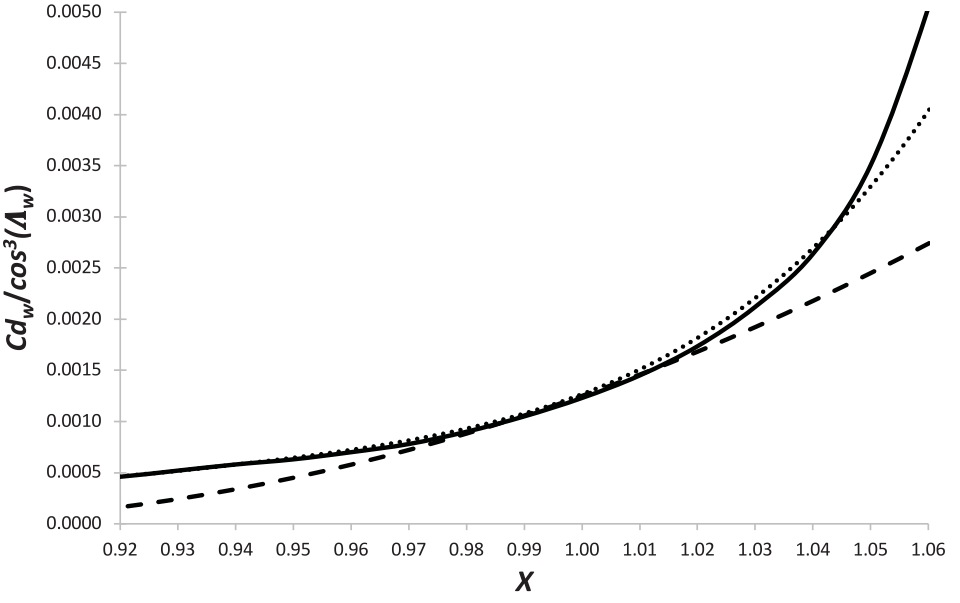

Figure 4. *The variation of wave drag coefficient with the characteristic parameter X - solid line is the original Shevell [8] curve, dotted line is Equation (36) and the dashed line is Equation (38) with j_1 and j_2 being set to 0.080 and 0.875, respectively.*

https://doi.org/10.1017/aer.2024.10 Published online by Cambridge University Press

For the analysis carried out in Poll and Schumann [5], Shevell's curve was represented by the relation

$$(Cd_w)_{creep} \approx cos^3(\Lambda_w)\left(0.016(X-0.75)^2\right), \tag{35}$$

for X less than 0.92 and for larger values

$$(Cd_w)_{rise} \approx cos^3(\Lambda_w)\left(0.016(X-0.75)^2 + 6.5(X-0.92)^4\right). \tag{36}$$

The form of the additional term in the drag "rise" variation was chosen to reflect the "ideal" drag rise due solely to the presence of a normal shock wave in the flow as derived by Lock [16], i.e.

$$(Cd_w)_{shock} \propto cos^3(\Lambda_w)\,(M_\infty \cos(\Lambda_w) - constant)^4. \tag{37}$$

Equation (36) is included in Fig. 4 and it is a reasonable approximation to the Shevell curve for values of X up to 1.05.

6.0 Estimation of the characteristics at the design optimum condition

Clearly, if an aircraft flies at a Mach number greater than the drag divergence Mach number of the wing's aerofoil sections, there will be a significant fuel penalty. Hence, in practice and mainly for reasons of economy, the largest operational value is usually the long-range cruise Mach number, M_{LRC}. Furthermore, Poll [3] (Equation (24)) has estimated that the Mach number for absolute minimum fuel burn, M_o, is about 3.5% lower than M_{LRC} and that the corresponding wave drag coefficient is less than 10 drag counts. This suggests that the optimum condition is likely to occur at the top end of the drag creep region, i.e. at a value of X that is close to unity. In this region, Equation (36) is both complex and not a particularly good match to the gradients of Shevell's original curve. Therefore, to simplify the analysis and improve the accuracy, the wave drag coefficient in the region of the optimum is given by the local approximation,

$$\frac{Cd_w}{cos^3(\Lambda_w)} \approx j_1(X-j_2)^2, \tag{38}$$

where j_1 and j_2 are constants. By matching the value and gradient of the Shevell curve when X is unity, j_1 and j_2 are found to be 0.080 and 0.875 respectively. This curve is also shown in Fig. 4 and the agreement is very good for X in the range 0.97 to 1.02.

Hence, using Equations (24) and (38), at the design condition,

$$\left(\frac{M_\infty}{Cd_w}\frac{\partial Cd_w}{\partial M_\infty}\right)_{DO} = 2(1-\delta_{DO})\left(\frac{X}{X-j_2}\right)_{DO} \tag{39}$$

and

$$\left(\frac{C_L}{Cd_w}\frac{\partial Cd_w}{\partial C_L}\right)_{DO} = \delta_{DO}\left(\frac{X}{X-j_2}\right)_{DO}, \tag{40}$$

where

$$\delta_{DO} = \frac{2(0.10)}{cos^2(\Lambda_w)}\left(\frac{C_L}{M_{CC}}\right)_{DO}. \tag{41}$$

Using Equations (A-15) and (A-16) from Appendix A, it can be shown that the optimum values of the lift coefficient and the wave drag coefficient are related directly, i.e.

$$\left(\frac{KC_L^2}{Cd_0}\right)_{DO} = \left(\frac{2(1-\delta_{DO}) + \delta_{DO}(2-\eta_2)}{2(1-\delta_{DO})\left(1+\left(\frac{k_1}{K}\right)b(1+\Gamma_{DO})\right) + \delta_{DO}\left(2+\eta_2+\left(\frac{k_1}{K}\right)b\right)}\right)\left(\frac{Cd_w}{Cd_0}\right)_{DO} +$$

$$\left(\frac{2(1-\delta_{DO})\,(1-b(1+\Gamma_{DO})) + \delta_{DO}(2-\eta_2-b)}{2(1-\delta_{DO})\left(1+\left(\frac{k_1}{K}\right)b(1+\Gamma_{DO})\right) + \delta_{DO}\left(2+\eta_2+\left(\frac{k_1}{K}\right)b\right)}\right). \tag{42}$$

https://doi.org/10.1017/aer.2024.10 Published online by Cambridge University Press

Since δ_{DO} depends upon $(C_L)_{DO}$, this is an implicit expression for $(C_L)_{DO}$ that can only be solved by iteration. Consequently, approximate solutions will be developed.

As shown in Appendix B, over the parameter ranges of practical interest, after some manipulation, further approximation and curve fitting, it is found that the wave drag coefficient is well represented by

$$\left(\frac{Cd_w}{Cd_0}\right)_{DO} \approx \left(\frac{\sigma^2}{j_1(j_2)^2}\right)\frac{(Cd_0)_{DO}}{cos^3(\Lambda_w)} \approx 16.3\sigma^2\frac{(Cd_0)_{DO}}{cos^3(\Lambda_w)}, \tag{43}$$

where j_1 and j_2 have been taken to be 0.080 and 0.875, respectively, and

$$\sigma \approx 0.44(2\eta_2 + b)\left(1 - \left(\frac{2+\eta_2}{2\eta_2+b}\right)b(1+\Gamma_{DO})\right). \tag{44}$$

This expression depends upon fixed characteristics of the aircraft and the engine, the Reynolds number at the design condition and the temperature lapse rate in the atmosphere. In addition, again to a good approximation, it is independent of δ_{DO}. Therefore, its accuracy is largely unaffected by the uncertainty in the values of the coefficients in Equation (34).

Combining Equations (38) and (43) gives

$$X_{DO} \approx j_2\left(1 + \frac{1}{\sigma}\left(\frac{Cd_w}{Cd_0}\right)_{DO}\right). \tag{45}$$

This is also approximately independent of δ_{DO}, with a 10% error in $(Cd_w)_{DO}$ changing X_{DO} by only about 1%. The optimum Mach number is given by

$$M_{DO} = \left(\frac{(M_{CC})_{DO}}{cos(\Lambda_w)}\right)X_{DO} \approx j_2\left(1 + \frac{1}{\sigma}\left(\frac{Cd_w}{Cd_0}\right)_{DO}\right)\left(\frac{(M_{CC})_{DO}}{cos(\Lambda_w)}\right), \tag{46}$$

but, since M_{DO} is proportional to $(M_{cc})_{DO}$, estimates for M_{DO} are subject to at least the same uncertainty as $(M_{cc})_{DO}$, i.e. ±7%. This is not accurate enough for practical applications. However, using public domain sources, Poll and Schumann [5] have obtained estimates for M_{DO}, whose maximum error is about ±4% and better than ±2% in most of the cases considered. Therefore, since more accurate values are already available, the lack of accuracy associated with Equation (46) does not present an insurmountable problem and M_{DO} can be treated as an input rather than an output.

In addition, from Equations (40) and (45),

$$\left(\frac{C_L}{Cd_w}\frac{\partial Cd_w}{\partial C_L}\right)_{DO} \approx \left(1 + \sigma\left(\frac{Cd_0}{Cd_w}\right)_{DO}\right)\delta_{DO}. \tag{47}$$

Hence, from Equations (24) and (25),

$$(C_L)_{DO} \approx \left(1 - \frac{1}{2}\left(b\left(1 + \left(\frac{k_1}{K}\right)\right)(1+\Gamma_{DO}) + \sigma\delta_{DO} - (1-\delta_{DO})\left(\frac{Cd_w}{Cd_0}\right)_{DO}\right)\right)\left(\frac{Cd_0}{K}\right)^{1/2}_{DO} \tag{48}$$

and

$$(Cd)_{DO} \approx 2\left(1 - \frac{1}{2}\left(b\left(1 + \left(\frac{k_1}{K}\right)\right)(1+\Gamma_{DO}) + \sigma\delta_{DO} - (2-\delta_{DO})\left(\frac{Cd_w}{Cd_0}\right)_{DO}\right)\right)(Cd_0)_{DO}. \tag{49}$$

Both these relations involve δ_{DO}, which is a function of $(C_L)_{DO}$ and the coefficients in Equation (34). However, it is easily shown that both $(C_L)_{DO}$ and $(Cd)_{DO}$ are also relatively insensitive to δ_{DO}, with a 10% error resulting in a change of less than 0.5% in either quantity, whilst a 10% error in $(Cd_w)_{DO}$ only changes $(C_L)_{DO}$ by about 0.25% and $(Cd)_{DO}$ by 0.5%. Therefore, using mid-range values and taking j_1 and j_2 to be 0.080 and 0.875, respectively,

$$(C_L)_{DO} \approx (0.985\,(1 - 0.60b(1+\Gamma_{DO})) \pm 0.010)\left(\frac{Cd_0}{K}\right)^{1/2}_{DO}, \tag{50}$$

https://doi.org/10.1017/aer.2024.10 Published online by Cambridge University Press

$$(Cd)_{DO} \approx 2(1.035\,(1-0.68b(1+\Gamma_{DO}))\ \pm 0.025\,)\,(Cd_0)_{DO} \tag{51}$$

and

$$\left(\frac{L}{D}\right)_{DO} \approx \frac{1}{2}\,(0.950\,(1+0.08b(1+\Gamma_{DO}))\ \pm 0.025\,)\left(\frac{1}{KCd_0}\right)^{1/2}_{DO}. \tag{52}$$

These "first-order" estimates are very simple, yet surprisingly accurate, and they reveal the fundamental character of the solution.

Using $(C_L)_{DO}$ from Equation (50), together with Equations (34) and (41), gives

$$\delta_{DO} \approx \frac{0.266}{\cos^2(\Lambda_w)}\left(1+\frac{0.133}{\cos^2(\Lambda_w)}\,(1-0.60b(1+\Gamma_{DO}))\left(\frac{Cd_0}{K}\right)^{\frac{1}{2}}_{DO}\right)\times \left((1-0.60b(1+\Gamma_{DO}))\left(\frac{Cd_0}{K}\right)^{1/2}_{DO}\right). \tag{53}$$

Substituting this result into Equations (48) and (49) gives accurate estimates for $(C_L)_{DO}$ and $(C_d)_{DO}$ that depend upon known aircraft geometric parameters and engine characteristics, plus $(Cd_0)_{DO}$, which in turn depends upon the, yet to be determined, Reynolds number, R^{ac}_{DO}.

At this stage, the presentation can be simplified by adopting the "ψ" notation originally introduced by Poll and Schumann [4, 5]. Therefore, at the design optimum condition,

$$M_{DO} = \psi_4 \tag{54}$$

and, using equation (A-6) from Appendix A, the Reynolds number may be written as

$$R^{ac}_{DO} = \frac{\psi_5}{\left(1+1.34\left(\overline{\Delta T}\right)_{DO}\right)}\left(\frac{(p_\infty)_{DO}}{(p_{TP})_{ISA}}\right)^{\iota_{DO}}, \tag{55}$$

where

$$\psi_5 = \left(\frac{S^{1/2}_{ref}\psi_4\gamma p_{TP}}{\mu_{TP}a_{TP}}\right)_{ISA}. \tag{56}$$

Whilst, from the definition of lift coefficient,

$$(C_L)_{DO} = \psi_6\left(\frac{m}{MTOM}\right)\left(\frac{(p_{TP})_{ISA}}{(p_\infty)_{DO}}\right) = \psi_6\left(\frac{m}{MTOM}\right)\left(\frac{\psi_5}{\left(1+1.34\left(\overline{\Delta T}\right)_{DO}\right)R^{ac}_{DO}}\right)^{\frac{1}{\iota_{DO}}}, \tag{57}$$

with

$$\psi_6 = \left(\frac{MTOM.g}{(\gamma/2)\,(p_{TP})_{ISA}\psi^2_4 S_{ref}}\right). \tag{58}$$

where *MTOM* is the aircraft's maximum permitted take-off mass. Also following Poll and Schumann [4] and as described in Appendix B, the variation of e_{LS} with C^{ac}_F may be approximated by a power law of the form

$$e_{LS} \approx \frac{E}{(C^{ac}_F)^{\tau}}. \tag{59}$$

However, in contrast to Poll and Schumann [4] and following Equation (50), the definition of ψ_2 is changed (slightly) from the original version to read

$$\psi_2 = \frac{(C_L)_{DO}}{(1-0.60b(1+\Gamma_{DO}))}\left(\frac{1}{C^{ac}_F}\right)^{\left(\frac{1-\tau}{2}\right)}_{DO}. \tag{60}$$

https://doi.org/10.1017/aer.2024.10 Published online by Cambridge University Press

Combining Equations (55), (57) and (60), the value of the mass ratio at which the design cruise coincides with the 226.32 *hPa* isobar, i.e. $(p_\infty)_{DO}$ equals $(p_{TP})_{ISA}$, is

$$\left(\frac{m}{MTOM}\right)_{(p_{TP})_{ISA}} \approx \left(1+\frac{b}{2}\left(1.34\left(1-\tau\right)\left(\overline{\Delta T}\right)_{DO}-1.20\left(1+\Gamma_{DO}\right)\right)\right)\psi_7, \tag{61}$$

where

$$\psi_7 = \frac{\psi_2}{\psi_6}\left(\frac{a}{\psi_5^b}\right)^{\left(\frac{1-\tau}{2}\right)}. \tag{62}$$

This simple result, which only depends upon input parameters, determines the value of ι_{DO}, since, when the mass ratio exceeds this value, $(p_\infty)_{DO}$ is more than 226.32 *hPa* and ι_{DO} is 0.74505. Conversely, if the mass ratio is less than, or equal to, this value, $(p_\infty)_{DO}$ is less than 226.32 *hPa* and ι_{DO} is equal to one.

The Reynolds number at the design condition is then found by combining Equations (57) and (60), eliminating $(C_L)_{DO}$ to give,

$$R_{DO}^{ac} \approx \frac{\psi_5}{\left(1+\kappa_{DO}\left(1.34\left(\overline{\Delta T}\right)_{DO}-0.60\iota_{DO}b(1+\Gamma_{DO})\right)\right)}\left(\frac{1}{\psi_7}\left(\frac{m}{MTOM}\right)\right)^{\iota_{DO}\kappa_{DO}}, \tag{63}$$

where

$$\kappa_{DO} = \left(\frac{2}{2-\iota_{DO}b(1-\tau)}\right). \tag{64}$$

Therefore, for a given aircraft weight, m, the design Reynolds number depends upon fixed aircraft characteristics and the design atmospheric parameters all of which are known.

Having obtained the Reynolds number, the skin friction coefficient is given by

$$\left(C_F^{ac}\right)_{DO} \approx \left(1+\kappa_{DO}b\left(1.34\left(\overline{\Delta T}\right)_{DO}-0.60\iota_{DO}b(1+\Gamma_{DO})\right)\right)\left(\frac{a}{\psi_5^b}\right)\left(\psi_7\left(\frac{MTOM}{m}\right)\right)^{\iota_{DO}\kappa_{DO}b}. \tag{65}$$

Since the Reynolds number is being raised to a power lying in the range 0.1 to 0.15, the use of Equation (50) to give $(C_L)_{DO}$ introduces an error in $\left(C_F^{ac}\right)_{DO}$ of less than 0.25%. Hence, an accurate approximate solution for $(Cd_0)_{DO}$ is obtained by using Equations (16) and (65) and values of $(Cd_w)_{DO}$ and δ_{DO} follow from Equations (43) and (53). Equations (46), (48) and (49) yield estimates for M_{DO}, $(C_L)_{DO}$ and $(Cd)_{DO}$ and, using Equations (26) and (52),

$$\left(\frac{L}{D}\right)_{DO} \approx \frac{1}{2}\left(1-\frac{1}{2}\left(\frac{Cd_w}{Cd_0}\right)_{DO}\right)\left(\frac{1}{KCd_0}\right)_{DO}^{1/2} \approx \left(1+0.08b(1+\Gamma_{DO})\right)\psi_3\left(\frac{1}{C_F^{ac}}\right)_{DO}^{\left(\frac{1+\tau}{2}\right)}. \tag{66}$$

Finally, using Equations (11) and (66), the design value of $(\eta_o L/D)$ is given by

$$(\eta_o L/D)_{DO} \approx (\eta_1 (M_{DO})^{\eta_2})\left(\frac{L}{D}\right)_{DO} = \left(1+0.08b(1+\Gamma_{DO})\right)\psi_1\left(\frac{1}{C_F^{ac}}\right)_{DO}^{\left(\frac{1+\tau}{2}\right)} \tag{67}$$

and, hence,

$$(\eta_o)_{DO} = \frac{\psi_1}{\psi_3}. \tag{68}$$

This completes the approximate solution for the design optimum condition.

7.0 Evaluating the characteristics at the design optimum

Although the actual design optimum conditions are known only to the aircraft manufacturer, for illustrative purposes, it is assumed that they correspond to operation in the *ISA* with the aircraft at 80% of its maximum permitted take-off mass, *MTOM*. This being the case, the input parameters are *MTOM*, the wing reference area, S_{ref}, span, s, quarter chord sweep angle, Λ_w, and whether, or not, winglets are fitted,

https://doi.org/10.1017/aer.2024.10 Published online by Cambridge University Press

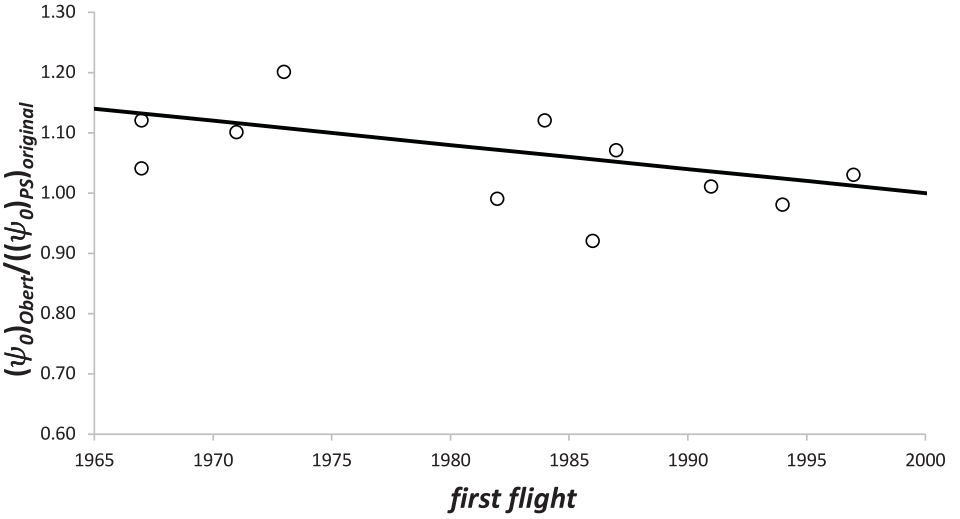

Figure 5. *The variation of the ψ_0 correction factor based upon data from Obert [15] with the date of the aircraft's first flight.*

the fuselage maximum width, b_f, plus the nominal engine bypass ratio, *BPR*, together with estimates for the zero-lift drag parameter, ψ_0 (Equation 16), M_{DO}, and $(\eta_o L/D)_{DO}$. As described in Poll and Schumann [5], ψ_0 is determined solely by the airframe geometry, which is relatively easy to find, whilst the most difficult parameters to estimate are M_{DO} and $(\eta_o L/D)_{DO}$. However, methods for obtaining these quantities from public domain sources are described in Poll and Schumann [5], which also contains complete data sets for 53 aircraft and engine combinations. In terms of the ψ parameters, ψ_1 is obtained from $(\eta_o L/D)_{DO}$ (Equation (67)), ψ_4 is equal to M_{DO} (Equation (54)), ψ_5 depends upon S_{ref} and ψ_4 (Equation (57)), ψ_6 depends upon $MTOM$, S_{ref} and ψ_4 (Equation (58)), i.e. they depend only upon the input parameters, whilst ψ_2, ψ_3 and ψ_7 are outputs. Since the various quantities at the design optimum conditions for a given aircraft only need to be computed once, in order to have accurate and self-consistent values, Equation (42) has been used to link $(C_L)_{DO}$ to δ_{DO} and solutions obtained by iteration.

The original data base was published some three years ago and, since that time, the values have been reviewed, refined and improved. This has resulted in some minor amendments and extensions being made and latest updated values are presented here.

As already noted, the calculation requires a knowledge of ψ_0. In Poll and Schumann [5] this parameter was obtained from information given Fig. 40.17 of Obert [15] and, as indicted in Fig. 1 of Ref. [5], these values are subject to an uncertainty of more than ±10%. However, Chapter 24 of Obert [15] contains additional information on the variation of drag with Mach number at fixed values of the lift coefficient for 11 of the aircraft types in the *PS* data base. These types are marked with an "*" in Table 1. In all, there are 31 values for the drag coefficient at a Mach number of about 0.5 for values of C_L between 0.3 and 0.5 and all lie within the expected range of validity of Equation (15). Since Equation (23) is well established, this was used to determine K, whilst ψ_0 was varied until the values for Cd given by Equation (16) were brought into best alignment with the Obert value for each aircraft. The resulting data set had an RMS deviation of about 1% and a maximum deviation of less than 2.5%. Ratios of the new ψ_0 to the original values were then plotted against the date of the aircraft's first flight and the result is given in Fig. 5.

Whilst the scatter is still about ±10 %, the data indicate that, for a given aircraft geometry, ψ_0 and, hence, $(Cd_0)_{DO}$, has been reducing steadily over time. Although not identified in Ref. (5), this trend is to be expected, since improved aerodynamic design has reduced the interference effects between

https://doi.org/10.1017/aer.2024.10 Published online by Cambridge University Press

Table 1. *Updated input data for a range of turbofan powered, civil transport aircraft. The "*" indicates that additional drag data is available in Obert [15]*

ICAO	*MTOM (kg)*	S_{ref} (m^2)	*s (m)*	Λ_w *(deg)*	*Winglets*	b_f *(m)*	*BPR*	ψ_0	M_{DO}	$(\eta L/D)_{DO}$
A30B*	165,000	260.0	44.83	28.0	no	5.64	4.6	8.774	0.753	4.642
A306	170,500	260.0	44.84	28.0	no	5.64	4.9	7.804	0.753	5.003
A310	138,600	219.0	43.89	28.0	no	5.64	5.0	8.376	0.772	5.544
A313	150,000	219.0	43.89	28.0	no	5.64	5.0	8.213	0.772	5.114
A318	68,000	122.4	34.10	25.0	no	3.95	5.2	7.471	0.753	5.447
A319	73,500	122.4	34.10	25.0	no	3.95	5.6	7.701	0.753	5.564
A320*	73,500	122.4	34.10	25.0	no	3.95	5.6	8.395	0.753	5.440
A321	89,000	122.4	34.15	25.0	no	3.95	5.3	8.631	0.753	5.376
A332	233,000	361.6	60.30	29.7	no	5.64	5.1	6.692	0.786	7.047
A333	233,000	361.6	60.30	29.7	no	5.64	5.1	6.900	0.786	6.712
A342*	257,000	361.6	60.30	29.7	no	5.64	6.7	7.077	0.786	6.861
A343	257,000	361.6	60.30	29.7	no	5.64	6.7	7.384	0.786	6.600
A345	372,000	437.3	63.45	31.1	no	5.64	7.5	6.731	0.796	7.144
A346	368,000	437.3	63.45	31.1	no	5.64	7.5	7.057	0.796	7.243
A359	275,000	445.0	64.75	32.0	no	5.96	9.0	6.140	0.820	8.302
A388	569,000	845.0	79.80	30.0	no	7.14	7.9	6.132	0.820	7.638
B712	54,884	92.8	28.40	25.0	no	3.40	4.6	8.722	0.724	4.211
B732*	52,390	99.0	28.35	25.0	no	3.76	1.0	8.406	0.685	3.499
B733*	61,236	102.0	28.90	25.0	no	3.76	5.1	9.200	0.729	4.251
B734	68,039	102.5	28.90	25.0	no	3.76	5.1	8.898	0.729	4.202
B735	60,555	103.7	28.90	25.0	no	3.76	5.1	8.335	0.729	4.197
B736	65,544	124.6	34.30	25.0	no	3.76	5.4	7.425	0.758	5.138
B737	70,080	124.6	34.30	25.0	no	3.76	5.2	7.611	0.758	5.195
B738*	79,016	124.6	34.30	25.0	no	3.76	5.1	8.182	0.758	5.106
B739	85,139	124.6	34.32	25.0	no	3.76	5.1	7.928	0.758	5.112
B742*	371,900	511.0	59.64	37.5	no	6.50	4.8	7.019	0.830	5.417
B743	377,800	511.0	59.64	38.5	no	6.50	4.8	6.882	0.830	5.505
B744	396,894	547.0	64.44	37.5	no	6.50	5.0	6.688	0.830	6.170
B748	442,253	594.0	68.40	37.5	no	6.50	8.0	6.249	0.830	7.133
B752*	113,400	189.0	38.06	25.0	no	3.76	4.7	7.102	0.772	5.585
B753	122,470	189.0	38.06	25.0	no	3.76	4.7	7.594	0.772	5.196
B762	179,169	283.3	47.57	31.5	no	5.03	4.9	6.963	0.772	6.294
B763*	158,758	283.3	47.57	31.5	no	5.03	4.9	6.297	0.772	6.156
B764	204,116	283.3	51.92	31.5	no	5.03	5.1	7.202	0.772	6.360
B77L	347,450	427.8	64.80	31.6	no	6.20	7.2	6.504	0.811	7.555
B772*	286,900	427.8	60.93	31.6	no	6.20	7.0	6.462	0.811	6.947
B77W	351,530	427.8	64.80	31.6	no	6.20	7.1	7.159	0.811	7.755
B773	299,370	427.8	60.93	31.6	no	6.20	6.3	7.069	0.811	6.812
B788	227,930	360.0	60.12	32.2	no	5.77	9.0	6.383	0.815	8.323
B789	254,011	360.0	60.12	32.2	no	5.77	9.0	6.478	0.815	8.279
E135	20,000	51.2	20.04	22.5	no	2.25	4.8	8.018	0.704	3.429
E145	22,000	51.2	20.04	22.5	no	2.25	4.7	8.380	0.704	3.686
E170	37,200	72.7	25.30	22.5	no	3.15	5.1	8.144	0.733	4.262
E195	48,790	92.5	27.73	22.5	no	3.00	5.1	8.034	0.758	4.551
MD82	67,812	112.3	32.85	22.5	no	3.35	1.7	8.956	0.753	4.106
MD83	72,575	112.3	32.85	22.5	no	3.35	1.7	8.856	0.753	4.319
GLF5	41,277	105.6	28.50	25.0	no	2.50	4.1	6.702	0.772	5.632

https://doi.org/10.1017/aer.2024.10 Published online by Cambridge University Press

Table 1. *Continued.*

ICAO	*MTOM* (kg)	S_{ref} (m^2)	s (m)	Λ_w (deg)	*Winglets*	b_f (m)	*BPR*	ψ_0	M_{DO}	$(\eta L/D)_{DO}$
CRJ9	38,329	76.2	23.25	26.0	no	2.69	5.1	7.351	0.753	4.460
DC93	48,988	93.0	28.44	24.0	no	3.35	1.0	7.952	0.733	3.359
RJ1H	44,225	77.3	26.34	15.0	no	3.50	5.1	9.769	0.676	3.318
B722*	83,820	157.9	32.92	32.0	no	3.76	1.0	7.902	0.830	3.844
A20N	79,000	122.4	35.10	25.0	yes	3.59	11.6	7.531	0.753	6.661
A21N	93,500	122.4	35.27	25.0	yes	3.95	11.6	8.035	0.753	5.962

the various components, including that between the wing and the engines, and improved manufacturing techniques have reduced excrescence drag and surface roughness. These new results suggest that, between 1970 and 2000, ψ_0 has decreased by about 15% and a "best fit" gives

$$\frac{\psi_0}{\left((\psi_0)_{PS}\right)_{original}} \approx 9.0 - 4.0\left(\frac{first\,flight}{1000}\right). \tag{69}$$

Hence, a small, but significant, improvement to the overall accuracy of the method can be achieved by applying a simple correction factor to the original values of ψ_0. Where the factor for a particular aircraft type is given by Obert, the Obert value is used. In all other cases, an estimate is obtained from Equation (69).

In Ref. (3), nominal values for bypass ratio were provided for specific engines. However, most aircraft can be fitted with more than one engine type and, in some instances, the precise engine type may not be known. Therefore, to cover the more general case, the average *BPR* for all engine types fitted to each aircraft type was obtained using the data provided in the ICAO engine data base [17]. These values were used to estimate η_2 via Equation (36) from Poll and Schumann [5]. The revised input values are given in Table 1.

The parameters ψ_4, ψ_5 and ψ_6 retain the values given in Poll and Schumann [5]. However, since their definitions have changed, the parameters τ, ψ_1, ψ_2, ψ_3 and ψ_7 must be recomputed.

The procedure began by obtaining initial estimates for τ and E using Equations (C-4) and (C-5) from Appendix C and giving $(Cd_0)_{DO}$ the mid-range value of 0.0175. An initial estimate for ψ_2 was obtained by combining Equations (16), (18), (50), (59) and (60) to give

$$\psi_2 \approx 0.985\sqrt{\pi.AR.E.\psi_0} \tag{70}$$

and an estimate for ψ_7 was then obtained from Equation (62). If the assumed value of $(m/MTOM)$ was less than, or equal to, ψ_7, the static pressure at cruise, $(p_\infty)_{DO}$, must be less than 226.32 hPa and ι_{DO} was set to unity, otherwise ι_{DO} was set to 0.74505. Furthermore, since the aircraft is operating in the *ISA*, Γ_{DO} is zero when ι_{DO} is unity, otherwise it is equal to -0.255. The initial estimate for R_{DO}^{ac} found from Equation (63), followed by $\left(C_F^{ac}\right)_{DO}$ and $(CD_0)_{DO}$ from Equations (16) and (17). The parameters $(k_1)_{DO}$ and $(k)_{DO}$ follow from Equations (22) and (23). Taking j_1 and j_2 to be 0.080 and 0.875, respectively, Equations (43) and (45) were then used to obtain $(Cd_w/Cd_0)_{DO}$ and X_{DO}. Since M_{DO} is assumed to be equal to the value of ψ_4 given in Poll and Schumann [5], from Equation (31)

$$(M_{CC})_{DO}^{ac} = \left(\frac{\psi_4 cos\,(\Lambda_w)}{X_{DO}}\right). \tag{71}$$

This was combined with $(C_L)_{DO}$ from Equation (60) to give δ_{DO} from Equation (41). In addition, this allows the estimation of a self-consistent value of the overall wing technology factor, $(M_{TF})^{ac}$, to be obtained from Equation (34), i.e.

$$(M_{TF})^{ac} = constant = (M_{CC})_{DO}^{ac} + 0.10\left(\frac{(C_L)_{DO}}{cos^2\,(\Lambda_w)}\right). \tag{72}$$

https://doi.org/10.1017/aer.2024.10 Published online by Cambridge University Press

At this point, the values of $(Cd_w/Cd_0)_{DO}$, δ_{DO}, ι_{DO} and η_2 were used to obtain an improved estimate for $(C_L)_{DO}$ from Equation (42). The value of $(p_\infty)_{DO}$ was then obtained from the definition of lift coefficient (Equation (5)). This was then used in Equation (55) to give a new value of R^{ac}_{DO} and in Equations (D-1) or (D-2) from Appendix D to give the corresponding flight level, $(FL)_{DO}$. The revised values of $(C_L)_{DO}$ and R^{ac}_{DO} were then used as input and the process repeated until full convergence was achieved. Corresponding values of τ, E, ψ_2 and ψ_7 were then obtained. It was found that the difference between the fully converged results and the initial estimates from the approximate solution was less than 2.5% for all parameters.

Finally, in Poll and Schumann [5] the values of ψ_1 were obtained by calibration using public domain information for $(\eta_o L/D)$. Therefore, since the definition of τ has changed, ψ_1 must also be recalculated to match these original values. The full set of results is given in Tables 2 and 3.

8.0 A Modified wave drag model

Shevell [8] assumes that there is a unique relationship between Cd_w and X, but, in practice, this is unlikely to be the case. However, since it is being assumed that the value of M_{DO} is known, Shevell's concept can be used to construct a "bespoke" wave drag model for each aircraft that has the correct behaviour at the design optimum condition.

The general expression for X is obtained by combining Equations (31), (34) and (71), i.e.

$$X = \frac{M_\infty cos\,(\Lambda_w)}{\left((M_{TF})^{ac} - 0.10\left(\frac{C_L}{cos^2(\Lambda_w)}\right)\right)} \tag{73}$$

and, in the immediate vicinity of the design optimum condition, the wave drag can be represented by a generalised form of equation (38), i.e.

$$\frac{Cd_w}{cos^3(\Lambda_w)} \approx j_1(X - j_2)^2. \tag{74}$$

Therefore, at the design optimum condition, combining this with Equation (40) gives

$$j_1 = \left(\frac{1}{\delta.X}\right)^2_{DO}\left(\frac{C_L}{Cd_0}\frac{\partial Cd_w}{\partial C_L}\right)^2_{DO}\left(\frac{Cd_0}{Cd_w}\right)_{DO}\left(\frac{(Cd_0)_{DO}}{cos^3(\Lambda_w)}\right) \tag{75}$$

and, hence,

$$j_2 = X_{DO} - \sqrt{\frac{1}{j_1}\left(\frac{Cd_w}{Cd_0}\right)_{DO}\left(\frac{(Cd_0)_{DO}}{cos^3(\Lambda_w)}\right)}. \tag{76}$$

If it is assumed that the Cd_w at the design condition is given by Equation (43), the corresponding lift coefficient can be found by iterative solution of Equation (42), using the approximate result given in Equation (50) as the first guess. This guarantees that all the conditions for the design optimum are met and the numerical values are self-consistent.

Using Equation (A-16) from Appendix A, the revised coefficients J_1 and J_2 are

$$j_1 = \frac{1}{16.3}\left(\frac{(1 - b(1+\Gamma)) + 16.3\sigma^2\frac{Cd_0}{cos^3(\Lambda_w)} - \left(1 + \left(\frac{k_1}{K}\right)b(1+\Gamma_{DO})\right)\left(\frac{KC_L^2}{Cd_0}\right)}{\sigma\delta X}\right)^2_{DO} \tag{77}$$

and

$$j_2 = X_{DO} - \sqrt{\frac{16.3}{j_1}}\left(\sigma\frac{(Cd_0)_{DO}}{cos^3(\Lambda_w)}\right). \tag{78}$$

Since J_1 and J_2 depend only upon aircraft and engine characteristics, these parameters are also characteristics of the aircraft-engine combination. Hence, J_1 and J_2 are included in Table 3.

https://doi.org/10.1017/aer.2024.10 Published online by Cambridge University Press

Table 2. *Estimates of the performance characteristics at the design condition (aircraft operating in the ISA with a mass of 80% MTOM)*

ICAO	M_{DO}	$(FL)_{DO}$	$(R^{ac})_{DO}$	$(M_{TF})^{ac}$	$(C_L)_{DO}$	$(L/D)_{DO}$	$(Cd)_{DO}$	$(\eta L/D)_{DO}$	J_1	J_2
A30B	0.753	358.5	9.25E+07	0.712	0.548	15.7	0.0350	4.642	0.074	0.868
A306	0.753	340.2	9.86E+07	0.721	0.519	16.9	0.0307	5.003	0.076	0.871
A310	0.772	373.1	8.14E+07	0.744	0.558	16.9	0.0329	5.544	0.073	0.869
A313	0.772	358.9	8.69E+07	0.738	0.564	17.2	0.0329	5.114	0.075	0.870
A318	0.753	392.0	5.42E+07	0.754	0.564	18.2	0.0309	5.447	0.075	0.871
A319	0.753	377.6	5.81E+07	0.755	0.569	18.0	0.0316	5.564	0.075	0.871
A320	0.753	385.4	5.59E+07	0.750	0.590	17.0	0.0347	5.440	0.073	0.869
A321	0.753	351.1	6.51E+07	0.740	0.606	16.9	0.0359	5.376	0.074	0.869
A332	0.786	365.8	1.10E+08	0.762	0.528	21.1	0.0250	7.047	0.076	0.872
A333	0.786	368.6	1.09E+08	0.761	0.535	20.7	0.0258	6.712	0.076	0.872
A342	0.786	354.3	1.16E+08	0.760	0.551	20.5	0.0268	6.861	0.077	0.872
A343	0.786	358.1	1.14E+08	0.757	0.561	20.0	0.0281	6.600	0.076	0.872
A345	0.796	305.2	1.53E+08	0.762	0.512	20.9	0.0245	7.144	0.078	0.874
A346	0.796	312.3	1.49E+08	0.759	0.523	20.3	0.0258	7.243	0.077	0.873
A359	0.820	377.8	1.21E+08	0.791	0.493	21.9	0.0225	8.302	0.078	0.874
A388	0.820	338.9	1.95E+08	0.794	0.446	20.6	0.0216	7.638	0.082	0.876
B712	0.724	369.0	5.06E+07	0.713	0.582	15.8	0.0367	4.211	0.072	0.867
B732	0.685	361.0	5.15E+07	0.665	0.555	15.5	0.0357	3.499	0.072	0.866
B733	0.729	367.4	5.39E+07	0.715	0.578	15.0	0.0384	4.251	0.072	0.867
B734	0.729	346.9	5.86E+07	0.710	0.579	15.4	0.0377	4.202	0.074	0.868
B735	0.729	362.9	5.55E+07	0.721	0.550	15.9	0.0346	4.197	0.074	0.870
B736	0.758	405.9	5.14E+07	0.759	0.564	18.2	0.0310	5.138	0.075	0.871
B737	0.758	393.4	5.46E+07	0.758	0.567	18.0	0.0315	5.195	0.075	0.871
B738	0.758	373.4	6.01E+07	0.754	0.581	17.4	0.0335	5.106	0.074	0.870
B739	0.758	359.3	6.42E+07	0.749	0.585	17.8	0.0330	5.112	0.075	0.871
B742	0.830	333.4	1.56E+08	0.707	0.459	17.7	0.0260	5.417	0.074	0.868
B743	0.830	327.6	1.59E+08	0.697	0.454	17.9	0.0254	5.505	0.073	0.867
B744	0.830	337.2	1.59E+08	0.714	0.466	19.0	0.0246	6.170	0.074	0.869
B748	0.830	327.7	1.72E+08	0.732	0.458	20.4	0.0224	7.133	0.077	0.872
B752	0.772	361.1	8.01E+07	0.770	0.497	17.8	0.0280	5.585	0.078	0.874
B753	0.772	354.5	8.20E+07	0.760	0.522	17.0	0.0306	5.196	0.078	0.873
B762	0.772	350.6	1.02E+08	0.719	0.500	18.4	0.0272	6.294	0.076	0.871
B763	0.772	362.7	9.73E+07	0.730	0.470	19.5	0.0240	6.156	0.077	0.873
B764	0.772	340.7	1.05E+08	0.723	0.544	19.5	0.0278	6.360	0.075	0.870
B77L	0.811	326.2	1.43E+08	0.772	0.519	21.7	0.0239	7.555	0.078	0.873
B772	0.811	356.7	1.29E+08	0.767	0.495	20.5	0.0242	6.947	0.078	0.874
B77W	0.811	332.6	1.40E+08	0.767	0.542	20.5	0.0264	7.755	0.076	0.872
B773	0.811	355.8	1.29E+08	0.760	0.515	19.4	0.0266	6.812	0.077	0.872
B788	0.815	380.4	1.06E+08	0.785	0.518	21.8	0.0238	8.323	0.077	0.873
B789	0.815	361.2	1.17E+08	0.785	0.518	21.8	0.0238	8.279	0.077	0.873
E135	0.704	436.9	2.64E+07	0.709	0.562	15.2	0.0370	3.429	0.074	0.869
E145	0.704	419.9	2.87E+07	0.706	0.570	14.9	0.0382	3.686	0.073	0.868
E170	0.733	403.7	3.84E+07	0.742	0.579	16.3	0.0355	4.262	0.074	0.870
E195	0.758	404.1	4.47E+07	0.765	0.560	16.3	0.0344	4.551	0.075	0.871
MD82	0.753	392.9	5.17E+07	0.744	0.616	16.2	0.0380	4.106	0.072	0.866

https://doi.org/10.1017/aer.2024.10 Published online by Cambridge University Press

Table 2. *Continued.*

ICAO	M_{DO}	$(FL)_{DO}$	$(R^{ac})_{DO}$	$(M_{TF})^{ac}$	$(C_L)_{DO}$	$(L/D)_{DO}$	$(Cd)_{DO}$	$(\eta L/D)_{DO}$	J_1	J_2
MD83	0.753	376.9	5.58E+07	0.745	0.610	16.4	0.0371	4.319	0.072	0.867
GLF5	0.772	453.9	3.83E+07	0.765	0.508	17.3	0.0293	5.632	0.077	0.873
CRJ9	0.753	389.3	4.33E+07	0.739	0.504	15.9	0.0316	4.460	0.076	0.872
DC93	0.733	392.7	4.58E+07	0.719	0.565	16.5	0.0343	3.359	0.074	0.868
RJ1H	0.676	361.8	4.47E+07	0.713	0.624	15.0	0.0417	3.318	0.073	0.869
B722	0.830	418.8	5.96E+07	0.734	0.504	15.1	0.0334	3.844	0.072	0.865
A20N	0.753	373.1	5.93E+07	0.786	0.598	19.8	0.0303	6.661	0.076	0.873
A21N	0.753	347.0	6.61E+07	0.777	0.625	19.2	0.0326	5.962	0.077	0.873

For values of X greater than X_{DO}, an additional term is required to capture the drag generated by strong shock waves. At this stage in the development of the model, it is proposed that the additional wave drag as X increases be represented by a variant of Equation (37), i.e.

$$\left(\frac{Cd_w}{cos^3(\Lambda_w)}\right)_{shock} \approx j_3(X - X_{DO})^4, \tag{79}$$

where j_3 is a constant that needs to be determined by calibration. However, initial indications are that j_3 is of order 100. Hence, for values of X greater than X_{DO}, the wave drag coefficient is given by

$$(Cd_w)_{rise} \approx cos^3(\Lambda_w)\left(j_1(X - j_2)^2 + j_3(X - X_{DO})^4\right). \tag{80}$$

This revised model allows the aircraft's lift-to-drag ratio to be estimated for any combination of Mach number and lift coefficient.

9.0 Updating the PS method

As described in Poll and Schumann [4, 5], application of the *PS* method for the estimation of the cruise values of $(\eta_o L/D)$ for any combination of mass, Mach number and flight level[7] requires a knowledge of the operational optimum conditions for $(\eta_o L/D)$ for the actual mass and the specific atmosphere being encountered. The operational optima are governed by Equations (8) and (9), whilst the design optimum is governed by Equations (13) and (14), and so, in general, the two conditions will not be the same. Whilst the full model described in the previous sections can always be used to determine the operational optimum, this will need to be done numerically. However, in practise, the differences between the design optimum and the operational optima are expected to be small and so, to a good approximation, operational optimum conditions may be expressed as perturbations of the design optimum values.

The estimation of the operational optimum begins by determining the value of the pressure variation parameter, i_{OO}, see Equation (A-7), in the actual atmosphere. Using Equation (61), if

$$\frac{m}{MTOM} > \left(\frac{m}{MTOM}\right)_{(p_{TP})_{ISA}} \approx \left(1 + \frac{b}{2}\left(1.34\,(1-\tau)\left(\overline{\Delta T}\right)_{OO} - 1.20\,(1+\Gamma_{OO})\right)\right)\psi_7, \tag{81}$$

ι_{OO} is equal to 0.74505, otherwise, ι_{OO} is equal to unity. Then, with m, $\left(\overline{\Delta T}\right)_{OO}$ and Γ_{OO} specified, using Equations (65), (60), (66) and (67),

$$\left(C_F^{ac}\right)_{OO} \approx \left(1 + \kappa_{OO} b\left(1.34\left(\overline{\Delta T}\right)_{OO} - 0.60\iota_{OO} b(1+\Gamma_{OO})\right)\right)\left(\frac{a}{\psi_5^b}\right)\left(\psi_7\left(\frac{MTOM}{m}\right)\right)^{\iota_{OO}\kappa_{OO}b}, \tag{82}$$

$$(C_L)_{OO} \approx (1 - 0.60b(1+\Gamma_{OO}))\,\psi_2\left(C_F^{ac}\right)_{OO}^{\left(\frac{1-\tau}{2}\right)}, \tag{83}$$

[7] Values must lie within the ranges of validity specified in Poll and Schumann [4, 5].

https://doi.org/10.1017/aer.2024.10 Published online by Cambridge University Press

Table 3. *Revised estimates of the* PS *characteristic parameters*

ICAO	τ	ψ_0	ψ_1	ψ_2	ψ_3	ψ_4	ψ_5	ψ_6	ψ_7	η_1	η_2
A30B	0.150	8.774	0.132	8.104	0.444	0.753	9.17E+07	0.693	0.844	0.346	0.545
A306	0.134	7.804	0.148	8.081	0.501	0.753	9.17E+07	0.716	0.777	0.344	0.538
A310	0.163	8.376	0.152	8.038	0.464	0.772	8.63E+07	0.657	0.923	0.376	0.536
A313	0.159	8.213	0.142	8.066	0.475	0.772	8.63E+07	0.711	0.845	0.343	0.537
A318	0.163	7.471	0.154	7.931	0.516	0.753	6.29E+07	0.607	1.005	0.348	0.532
A319	0.166	7.701	0.155	7.962	0.503	0.753	6.29E+07	0.656	0.942	0.358	0.522
A320	0.179	8.395	0.146	7.924	0.459	0.753	6.29E+07	0.656	0.976	0.370	0.522
A321	0.180	8.631	0.143	7.989	0.449	0.753	6.29E+07	0.794	0.816	0.369	0.528
A332	0.149	6.692	0.197	8.088	0.590	0.786	1.13E+08	0.645	0.893	0.379	0.535
A333	0.153	6.900	0.185	8.087	0.572	0.786	1.13E+08	0.645	0.904	0.368	0.534
A342	0.156	7.077	0.188	8.110	0.562	0.786	1.13E+08	0.711	0.828	0.376	0.498
A343	0.161	7.384	0.177	8.103	0.537	0.786	1.13E+08	0.711	0.843	0.372	0.498
A345	0.135	6.731	0.204	8.159	0.595	0.796	1.26E+08	0.831	0.665	0.382	0.479
A346	0.141	7.057	0.203	8.169	0.568	0.796	1.26E+08	0.822	0.686	0.399	0.479
A359	0.132	6.140	0.243	8.013	0.641	0.820	1.31E+08	0.569	0.943	0.413	0.445
A388	0.100	6.132	0.238	8.055	0.644	0.820	1.80E+08	0.620	0.773	0.406	0.470
B712	0.174	8.722	0.116	7.893	0.437	0.724	5.26E+07	0.699	0.906	0.317	0.545
B732	0.158	8.406	0.101	7.911	0.449	0.685	5.15E+07	0.698	0.868	0.285	0.627
B733	0.171	9.200	0.118	7.940	0.416	0.729	5.56E+07	0.700	0.899	0.335	0.534
B734	0.164	8.898	0.118	7.984	0.433	0.729	5.57E+07	0.774	0.801	0.324	0.534
B735	0.154	8.335	0.122	7.957	0.462	0.729	5.60E+07	0.681	0.881	0.313	0.534
B736	0.163	7.425	0.146	7.910	0.518	0.758	6.39E+07	0.567	1.071	0.327	0.527
B737	0.165	7.611	0.146	7.937	0.507	0.758	6.39E+07	0.607	1.012	0.334	0.531
B738	0.173	8.182	0.139	7.973	0.473	0.758	6.39E+07	0.684	0.924	0.341	0.533
B739	0.168	7.928	0.141	8.007	0.490	0.758	6.39E+07	0.737	0.847	0.334	0.533
B742	0.115	7.019	0.164	7.819	0.536	0.830	1.42E+08	0.654	0.754	0.339	0.541
B743	0.113	6.882	0.167	7.769	0.543	0.830	1.42E+08	0.664	0.734	0.341	0.542
B744	0.119	6.688	0.185	7.844	0.567	0.830	1.47E+08	0.652	0.766	0.360	0.537
B748	0.115	6.249	0.215	7.836	0.614	0.830	1.53E+08	0.669	0.735	0.382	0.468
B752	0.125	7.102	0.173	8.043	0.548	0.772	8.02E+07	0.623	0.870	0.362	0.542
B753	0.132	7.594	0.157	8.097	0.516	0.772	8.02E+07	0.673	0.829	0.351	0.542
B762	0.129	6.963	0.189	7.928	0.552	0.772	9.81E+07	0.657	0.814	0.393	0.538
B763	0.119	6.297	0.191	7.842	0.605	0.772	9.81E+07	0.582	0.880	0.362	0.538
B764	0.154	7.202	0.176	7.991	0.540	0.772	9.81E+07	0.748	0.779	0.374	0.534
B77L	0.140	6.504	0.213	8.121	0.613	0.811	1.27E+08	0.765	0.730	0.385	0.486
B772	0.127	6.462	0.206	8.024	0.608	0.811	1.27E+08	0.632	0.837	0.376	0.490
B77W	0.152	7.159	0.211	8.136	0.557	0.811	1.27E+08	0.774	0.751	0.420	0.489
B773	0.137	7.069	0.196	8.079	0.557	0.811	1.27E+08	0.659	0.834	0.391	0.507
B788	0.146	6.383	0.235	7.984	0.615	0.815	1.17E+08	0.589	0.954	0.418	0.445
B789	0.147	6.478	0.232	8.029	0.610	0.815	1.17E+08	0.657	0.861	0.417	0.445
E135	0.158	8.018	0.105	7.691	0.463	0.704	3.81E+07	0.487	1.232	0.273	0.541
E145	0.163	8.380	0.110	7.732	0.445	0.704	3.81E+07	0.536	1.141	0.299	0.543
E170	0.168	8.144	0.122	7.858	0.468	0.733	4.72E+07	0.589	1.060	0.309	0.533
E195	0.157	8.034	0.134	7.947	0.478	0.758	5.50E+07	0.569	1.062	0.324	0.534
MD82	0.190	8.956	0.107	7.947	0.424	0.753	6.03E+07	0.660	1.010	0.301	0.611
MD83	0.187	8.856	0.113	7.993	0.432	0.753	6.03E+07	0.706	0.939	0.313	0.611
GLF5	0.131	6.702	0.181	7.727	0.557	0.772	5.99E+07	0.406	1.329	0.376	0.558

https://doi.org/10.1017/aer.2024.10 Published online by Cambridge University Press

Table 3. *Continued.*

ICAO	τ	ψ_0	ψ_1	ψ_2	ψ_3	ψ_4	ψ_5	ψ_6	ψ_7	η_1	η_2
CRJ9	0.130	7.351	0.142	7.750	0.509	0.753	4.96E+07	0.550	0.993	0.325	0.533
DC93	0.162	7.952	0.097	7.907	0.475	0.733	5.34E+07	0.606	1.009	0.248	0.627
RJ1H	0.187	9.769	0.089	8.058	0.400	0.676	4.49E+07	0.776	0.877	0.274	0.534
B722	0.135	7.902	0.118	7.776	0.463	0.830	7.88E+07	0.477	1.134	0.286	0.627
A20N	0.184	7.531	0.176	7.930	0.521	0.753	6.29E+07	0.705	0.923	0.376	0.385
A21N	0.193	8.035	0.152	7.934	0.490	0.753	6.29E+07	0.835	0.801	0.347	0.385

$$\left(\frac{L}{D}\right)_{OO} \approx (1 + 0.08b(1 + \Gamma_{OO}))\ \psi_3 \left(\frac{1}{C_F^{ac}}\right)_{OO}^{\left(\frac{1+\tau}{2}\right)} \tag{84}$$

and

$$(\eta_o L/D)_{OO} \approx (1 + 0.08b(1 + \Gamma_{OO}))\ \psi_1 \left(\frac{1}{C_F^{ac}}\right)_{OO}^{\left(\frac{1+\tau}{2}\right)}. \tag{85}$$

Finally, Equation (46) is used to provide a correction to the Mach number,

$$M_{OO} \approx \psi_4 \left(1 - \frac{0.10}{cos^2\ (\Lambda_w)} \left(\frac{(C_L)_{OO} - (C_L)_{DO}}{(M_{CC})_{DO}}\right)\right). \tag{86}$$

In the Poll and Schumann [4, 5] method, ψ_1, ψ_2, and ψ_3 are assumed to be constant. However, the solutions developed here, specifically Equations (60), (66) and (67), show that these parameters are Reynolds number dependent. This dependency is both direct and indirect, but, in all cases, it is very weak. Therefore, if these parameters are evaluated at the design condition, they may be taken to be constant without any significant loss of accuracy. The relevant values of ψ_1, ψ_2 and ψ_3 are those listed in Table 3.

10. Discussion

As noted in the previous section, Poll and Schumann [5] have already obtained estimates for M_{DO} $(=\psi_4)$ that are adequate for practical application. These can be compared with the estimates obtained using the present approach and the results are given in Fig. 6. The estimates and the data correlate extremely well, but the scatter is $\pm 6\%$, which is about the expected level due to the uncertainty in the value of intercept in Equation (34). Hence, estimates for M_{DO} can only be improved by improving the accuracy of $(M_{cc})_{DO}$ and this requires detail that is unlikely to ever appear in the open literature.

In the current approach, the Poll and Schumann [5] estimates for M_{DO} are combined with the (accurate) estimates of X_{DO} from Equation (45) to obtain a value of $(M_{cc})_{DO}$ for each aircraft, i.e.

$$(M_{CC})_{DO}^{ac} = \frac{M_{DO} cos(\Lambda_w)}{X_{DO}}. \tag{87}$$

A "least squares" fit to the resulting values gives

$$(M_{CC})_{DO}^{ac} \approx 0.75 - 0.10 \left(\frac{(C_L)_{DO}}{cos^2\ (\Lambda_w)}\right). \tag{88}$$

The close agreement between this result and Equation (34) is a very strong indication that the drag estimates are accurate, but, as already noted, the intrinsic uncertainty is too great for a combination of Equations (46) and either (34) or (88) to yield satisfactory estimates for M_{DO}.

Apart from M_{DO} and, consequently, δ_{DO}, the uncertainty associated with all the other parameters is very small. The principal finding, and the result upon which the estimates are based, is the estimate

https://doi.org/10.1017/aer.2024.10 Published online by Cambridge University Press

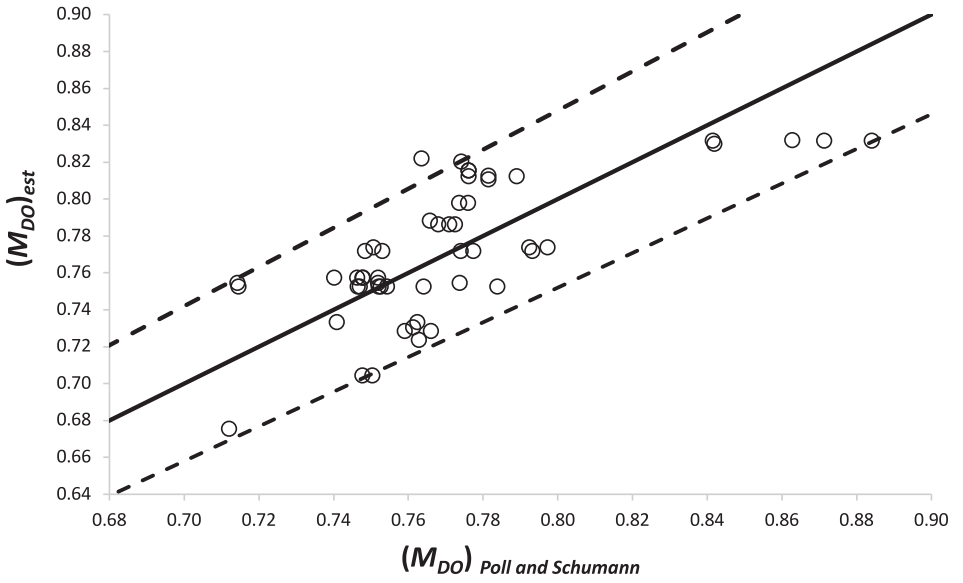

Figure 6. *Comparison of the estimates of the optimum Mach number with the values given by Poll and Schumann [5]. The dashed lines indicate a deviation of ±6%.*

for the Reynolds number at the design optimum ($\eta_o L/D$) – see Equation (63). This depends upon the aircraft's geometry, the instantaneous aircraft mass, m, and the properties of the atmosphere. Once this quantity is determined, the zero-lift drag coefficient, $(Cd_0)_{DO}$ and the lift-dependent drag factor, K_{DO}, follow immediately from Equations (16), (17) and (23). The second key result is the expression for the wave drag coefficient at the design optimum as given in Equation (43), i.e.

$$(Cd_w)_{DO} \approx 3.2\left((2\eta_2 + b)\left(1 - \left(\frac{2+\eta_2}{2\eta_2 + b}\right) b(1+\Gamma_{DO})\right)\right)^2 \left(\frac{(Cd_0)^2}{cos^3(\Lambda_w)}\right)_{DO}. \tag{89}$$

Taking mid-range values for the various parameters, a typical value for $(Cd_w)_{DO}$ is found to be about 8 drag counts or 2.5% of the total drag. This in consistent with statements in Torenbeek [9] that "*compressibility drag in fuel economical flight is typically between 5 and 10 counts*" or about 3% of the total – see Fig. 14.6 of Ref. (9). The wave drag coefficient is found to increases as $(Cd_0)_{DO}$ squared and also as almost η_2 squared. Consequently, aircraft with a smaller wing area per passenger and using low bypass ratio engines will have the highest values of wave drag at the optimum condition. This situation is typical of the older, short haul, single aisle aircraft. Conversely, long haul, twin aisle aircraft with large wing area per passenger and high bypass ratio engines will have low values. The wave drag also depends upon both the local temperature and the lapse rate.

The approximate solution also allows the effects of compressibility and variable Reynolds number on the maximum value of the lift-to-drag ratio and the lift coefficient and Mach number at which it occurs to be identified. As shown, in general, the results may be expressed as

$$\left(\frac{L}{D}\right)_{DO} \propto \frac{1}{2}\left(\frac{1}{KCd_0}\right)^{1/2}_{DO},\ (C_L)_{DO} \propto \left(\frac{Cd_0}{K}\right)^{1/2}_{DO} \text{ and } (Cd)_{DO} \propto 2(Cd_0)_{DO}. \tag{90}$$

When the Reynolds number is constant, i.e. changes in speed and altitude do not change Reynolds number, and there is no wave drag, the constants of proportionality are all unity.

As shown in Equations (50), (51) and (52), when both wave drag and Reynolds number variation are present and the aircraft is flying in the International Standard Atmosphere, the constants of proportionality for flight in the troposphere are found to be about 0.96 for $(L/D)_{DO}$, 0.92 for $(C_L)_{DO}$ and 0.96 for

https://doi.org/10.1017/aer.2024.10 Published online by Cambridge University Press

$(Cd)_{DO}$, whilst in the stratosphere the constants are 0.96, 0.90 and 0.94, respectively. In all cases, the constants are less than unity. The lowest values occur in the stratosphere and the impact upon $(C_L)_{DO}$ is largest with a reduction of 10%, followed by $(Cd)_{DO}$ with 6% and then $(L/D)_{DO}$ with 4%. These are significant changes, particularly for $(C_L)_{DO}$.

The reduction in $(C_L)_{DO}$ means that, for an aircraft of given mass flying at the optimum Mach number, the optimum flight level will be reduced relative to the constant Reynolds number, zero wave drag case. In Poll [3] it was found that, in the vicinity of the ISA tropopause,

$$\frac{d(FL)}{FL} \approx -0.61\frac{dp_\infty}{p_\infty} = 0.61\frac{d(C_L)_{DO}}{(C_L)_{DO}}. \tag{91}$$

Hence, for flight in the troposphere, the reduction in cruise altitude due to compressibility and Reynolds number variation is about 1,750 feet. When the aircraft leaves the troposphere and enters the stratosphere, $(C_L)_{DO}$ drops by an additional 2%, giving a further reduction of about 450 feet.

The approximate solution also allows the separation of the compressibility and Reynolds number effects. Reynolds number variation is removed by setting the constant b equal to zero. In this case, the constants of proportionality are the same for flight in both troposphere and stratosphere, becoming 0.95 for $(L/D)_{DO}$, 0.985 for $(C_L)_{DO}$ and 1.035 for $(Cd)_{DO}$. Therefore, through compressibility effects alone, $(L/D)_{DO}$ is reduced by about 5% and $(C_L)_{DO}$ is reduced by just 1.5%, whilst $(Cd)_{DO}$ is increased by 3.5%. Consequently, compressibility effects alone would account for a reduction in cruise altitude of only about FL 3.5, or 350 feet. The conclusion is that $(L/D)_{DO}$ is controlled primarily by compressibility effects, as shown in Equation (42), whilst the values of C_L and Cd at the design condition are largely determined by the Reynolds number variation, i.e. by the value of the coefficient b.

Generally, the surface of an aircraft is never perfectly smooth and in the early days of civil jet transport the surface quality could deteriorate quite quickly in routine operations. In extreme cases, the surface could become "aerodynamically rough", with the drag coefficient being a constant determined by the scale of the roughness, see, e.g. Obert [15] (Chapter 40). In this case, b is zero. As indicated in Equations (50) to (52), in this situation, the changes to $(L/D)_{DO}$, $(C_L)_{DO}$ and $(Cd)_{DO}$ are both relatively small and have no dependence upon the nature of the atmosphere. Since most of the standard texts on aircraft performance were written many years ago, this may explain why the effects of wave drag receive so little attention. More recently, with the progressive improvement in manufacturing processes and the development of better paints, modern surfaces tend to be "aerodynamically smooth", but with the boundary layers on the wing and fuselage usually still in the fully turbulent state, i.e. b is about 0.14.

Looking to the future, one of the most effective ways to reduce fuel consumption is to produce aircraft that can support extensive areas of laminar flow on the wing, the empennage and, possibly, the fuselage. This is because advanced materials and manufacturing techniques can now deliver extremely smooth surfaces with very few, or no, steps, or gaps, and very small waviness. These surfaces can also be perforated to allow the use of weak, surface suction to increase the stability of the laminar boundary layer and delay transition to turbulence to higher Reynolds numbers. The first generation of these aircraft are likely to see a 10% to 15% reduction in the Cd_0 resulting from limited regions of laminar flow on the wings and empennage and, from Equation (52), this will give a 5 to 7.5% increase in $(L/D)_{DO}$, with a corresponding reduction in the required fuel flow rate. However, as can be seen from Equation (50), this change in Cd_0 also reduces $(C_L)_{DO}$ by 5% to 7.5%, corresponding to a reduction in the optimum cruise altitude of between 1000 and 1500 feet. Furthermore, the existence of any regions of laminar flow will increase the value of the coefficient, b, in the skin friction law (Equation (17)). This is because, in pure laminar flow, b is equal to 0.5 – see Shevell [8]. Therefore, as the area covered by laminar flow increases and that covered by turbulent flow decreases, b must increase progressively from the current value of 0.14 to 0.5 and the constant of proportionality in Equation (50) will drop from about 0.9 to about 0.7. The combined effects of a reduction in Cd_0 and an increase in b will produce a significant lowering of the design optimum and, hence, the operational optimum cruise altitudes for these "advanced" aircraft. In addition, for a given aircraft, the improvement in $(L/D)_{DO}$ reduces the fuel required and, hence, the operational mass of the aircraft. This increases the optimum cruise altitude. However, it is demonstrated

https://doi.org/10.1017/aer.2024.10 Published online by Cambridge University Press

in Appendix E that, all other things being equal, the reduction in $(C_L)_{DO}$ is always the dominant effect. Consequently, the application of drag reducing technology to lower Cd_0 will always reduce the optimum cruise altitude.

Up to the present time, the evolutionary trend has been one of incremental improvements in engine overall efficiency and increases in airframe aerodynamic efficiency – through higher wing aspect ratios and small reductions in Cd_0 – see Poll [18]. The primary impact has been reduced trip fuel and the net effect is that optimum cruise altitudes have been rising slowly over time. The potential reversal of this trend by the introduction of novel technologies may have implications for the aircraft's environmental impact and deserves further consideration.

11.0 Conclusions

A turbofan powered, civil transport aircraft, with a specified weight and operating in a specified atmosphere, has its lowest possible fuel burn at a particular value of Mach number and flight level. These optimum operating conditions are governed by two partial differential equations, involving characteristics of both airframe and engine. However, for fixed Mach number cruise, the airframe lift-drag ratio and the engine overall efficiency both exhibit local maxima with respect to drag and, hence, thrust. Consequently, an absolute optimum is obtained when both parameters peak at the same Mach number and flight level. It is shown that this "perfect" matching of components can only be achieved at one particular set of conditions, termed the "design optimum" and the corresponding Mach number and flight level are fundamental characteristics of the aircraft-engine combination. Consequently, the governing differential equations for the general optimum have been used to describe the design optimum conditions in a completely general atmosphere. An approximate solution has been developed using established aerodynamic theory and a simple, aircraft bespoke, wave drag model that also allows the wave drag to be estimated at Mach numbers and flight levels far removed from the design optimum values. The solution has been used to estimate the influence of compressibility and Reynolds number both collectively and separately. Relative to the "classic text book" situation with constant Reynolds number and zero wave drag, it is found that L/D at the design optimum is hardly affected by changes in Reynolds number, but it is reduced by about 5% due to compressibility effects. Conversely, the corresponding values of lift and drag coefficients are reduced by about 10% and 6% respectively, primarily, due to variations in Reynolds number. Therefore, the effect of Reynolds number variation due to changes in flight level is significant.

In general, the flight conditions for the operating optimum will not be the same as the design optimum due to differences in aircraft weight and atmospheric conditions. However, since these variations are generally small, it has been possible to adapt a previously published method to estimate the optimum operating conditions for any aircraft weight and any atmospheric conditions, using the design optimum condition as the datum case.

Finally, some small changes have been made to previously published coefficients to improve the accuracy of the estimates. The revised parameter values are given in tabular form.

Looking ahead, comparisons are being conducted between the PS model and a number of sets of data from open sources, plus a few observations from other models. Preliminary results indicate that differences between the PS model and specific data sets can be largely removed by minor adjustments to some of the input parameters, but no changes to the model structure are required.

References

[1] Eurocontrol, Base of Aircraft Data (BADA), https://www.eurocontrol.int/model/bada

[2] Lissys, PIANO, https://www.lissys.uk

[3] Poll, D.I.A. On the relationship between non-optimum operations and fuel requirement for large civil transport aircraft, with reference to environmental impact and contrail avoidance strategy, *Aeronaut. J.*, December 2018, **122**, (1258), pp 1827–1870.

https://doi.org/10.1017/aer.2024.10 Published online by Cambridge University Press

[4] Poll, D.I.A. and Schumann, U. An estimation method for the fuel burn and other performance characteristics of civil transport aircraft in the cruise. Part 1 Fundamental quantities and governing relations for a general atmosphere, *Aeronaut. J.*, February 2021, **125**, (1284), pp 257–295.
[5] Poll, D.I.A. and Schumann, U. An estimation method for the fuel burn and other performance characteristics of civil transport aircraft in the cruise. Part 2 Determining the aircraft's characteristic parameters, *Aeronaut. J.*, February 2021, **125**, (1284), pp 296–340.
[6] ICAO, Manual of the ICAO Standard Atmosphere. ICAO Document No. 7488, 2nd Edition, 1964.
[7] Jenkinson, L.R., Simpkin, P. and Rhodes, D. Civil jet aircraft design, Arnold, 1999, ISBN: 0-340-74152-X.
[8] Shevell, R.S. *Fundamentals of flight*, 2nd edition, Prentice Hall, 1989. ISBN: 0-13-339060-8.
[9] Torenbeek, E. *Advanced Aircraft Design – Conceptual design, analysis and optimisation of subsonic civil aeroplanes*. John Wiley and Sons, Chichester, West Sussex, UK, 2013, ISBN: 9781119969303.
[10] Shevell, R.S. and Bayan F.P. Development of a method for predicting the drag divergence Mach number and the drag due to compressibility for conventional and supercritical wings, SUDAAR 552 (NASA Ames Research Centre Grant number NAG 2-18), Department of Aeronautics and Astronautics, Stanford University, July 1980.
[11] Shevell, R.S. Aerodynamic anomalies: Can CFD prevent or correct them? *Journal of Aircraft*, August 1986, **23**, (8), pp 641–649.
[12] Raymer, D.P. *Aircraft Design: A Conceptual Approach*, AIAA Educational Series, 1989, ISBN: 0-930403-51-7.
[13] Mason, W.H. Analytic models for technology integration in aircraft design, AIAA Paper 90-3262, September 1990.
[14] Boppe, C.W. CFD drag prediction for aerodynamic design. AGARD-AR-256, June 1989.
[15] Obert, E. *Aerodynamic Design of Transport Aircraft*, Delft University Press, 2009, ISBN: 978-1-58603-970-7.
[16] Lock, C.N.H. The ideal drag due to a shock, ARC R&M 2512, HMSO, 1951.
[17] ICAO engine data bank EASA, 2018. ICAO Engine Emissions Databank https://www.easa.europa.eu/easa-and-you/environment/icao-aircraft-engine-emissions-databank
[18] Poll, D.I.A. On the application of light weight materials to improve aircraft fuel burn – reduce weight or improve aerodynamic efficiency? *Aeronaut. J.*, **118**, (1206), August 2014, pp 903–934.

Appendix A. Estimation of the lift and drag coefficients at the design optimum condition.

Differentiation of the drag polar shown in Equation (15) gives

$$\frac{M_\infty}{Cd}\frac{\partial Cd}{\partial M_\infty} = \frac{Cd_0}{Cd}\left(\left(\frac{M_\infty}{Cd_0}\frac{\partial Cd_0}{\partial M_\infty}\right) - \left(4 - \left(\frac{M_\infty}{K}\frac{\partial K}{\partial M_\infty}\right)\right)\left(\frac{KC_L^2}{Cd_0}\right) + \left(\frac{M_\infty}{Cd_0}\frac{\partial Cd_w}{\partial M_\infty}\right)\right) \tag{A-1}$$

and

$$\frac{C_L}{Cd}\frac{\partial Cd}{\partial C_L} = \frac{Cd_0}{Cd}\left(\left(\frac{C_L}{Cd_o}\frac{\partial Cd_0}{\partial C_L}\right) + \left(2 + \left(\frac{C_L}{K}\frac{\partial K}{\partial C_L}\right)\right)\left(\frac{KC_L^2}{Cd_0}\right) + \left(\frac{C_L}{Cd_0}\frac{\partial Cd_w}{\partial C_L}\right)\right). \tag{A-2}$$

Using Equations (16) and (17),

$$\left(\frac{R^{ac}}{Cd_0}\frac{dCd_0}{dR^{ac}}\right) = -b = -0.14 \tag{A-3}$$

and, from Equation (4),

$$R^{ac} = S_{ref}^{1/2}\left(\frac{\gamma p_{TP}}{\mu_{TP}a_{TP}}\right)_{ISA}\left(\frac{p_\infty}{(p_{TP})_{ISA}}\right)\left(\frac{M_\infty}{\phi}\right), \tag{A-4}$$

where the subscript *TP* refers to conditions at the tropopause. Furthermore, as shown by Poll and Schumann [4], in a general atmosphere,

$$\phi = \frac{\mu_\infty a_\infty}{(\mu_{TP}a_{TP})_{ISA}} \approx \left(\frac{T_\infty}{(T_{TP})_{ISA}}\right)^{1.34} \approx \left(1 + 1.34\frac{\Delta T}{(T_{TP})_{ISA}}\right)\left(\frac{T_\infty}{T_{TP}}\right)_{ISA}^{1.34} \approx \left(1 + 1.34\overline{\Delta T}\right)\left(\frac{(p_{TP})_{ISA}}{p_\infty}\right)^{1.34\omega}. \tag{A-5}$$

where ΔT is the difference between the actual temperature and the temperature in the International Standard Atmosphere [1] at the same flight level and ω is a constant. Hence,

$$R^{ac} = S_{ref}^{1/2}\left(\frac{\gamma p_{TP}}{\mu_{TP}a_{TP}}\right)_{ISA}\left(\frac{M_\infty}{1 + 1.34\overline{\Delta T}}\right)\left(\frac{p_\infty}{(p_{TP})_{ISA}}\right)^{i}, \tag{A-6}$$

https://doi.org/10.1017/aer.2024.10 Published online by Cambridge University Press

with

$$\iota = 1 + 1.34\omega. \tag{A-7}$$

If p_∞ is greater than, or equal to, $(p_{TP})_{ISA}$, i.e. $p_\infty \geq 226.32\ hPa$, ω is -0.19026 and ι is 0.74505 and, if p_∞ is less than $(p_{TP})_{ISA}$, ω is zero and ι is equal to one. In addition, when the Mach number is constant,

$$\left(\frac{p_\infty}{R^{ac}}\frac{\partial R^{ac}}{\partial p_\infty}\right) = 1 - \left(\frac{p_\infty}{\phi}\frac{\partial \phi}{\partial p_\infty}\right) = 1 + \Gamma. \tag{A-8}$$

In the special case of the International Standard Atmosphere,

$$\Gamma \approx \iota - 1 = 1.34\omega, \tag{A-9}$$

whilst, in a completely general atmosphere, as demonstrated in Poll and Schumann [4],

$$\Gamma \approx 277\left(1 - \overline{\Delta T}\right)\left(\frac{1}{(T_{TP})_{ISA}}\frac{d_\infty}{dL}\right). \tag{A-10}$$

Hence, from Equations (7), (A-3), (A-4) and (A-8),

$$\left(\frac{M_\infty}{Cd_0}\frac{\partial Cd_0}{\partial M_\infty}\right) = -b \text{ and } \left(\frac{C_L}{Cd_o}\frac{\partial Cd_0}{\partial C_L}\right) = b(1+\Gamma)\ . \tag{A-11}$$

Also, from Equations (22) and (23),

$$\left(\frac{C_L}{K}\frac{\partial K}{\partial C_L}\right) = \frac{k_1}{K}\left(\frac{C_L}{Cd_o}\frac{\partial Cd_0}{\partial C_L}\right) \text{ and } \left(\frac{M_\infty}{K}\frac{\partial K}{\partial M_\infty}\right) = \frac{k_1}{K}\left(\frac{M_\infty}{Cd_0}\frac{\partial Cd_0}{\partial M_\infty}\right)\ . \tag{A-12}$$

Equations (A-1) and (A-2) then become

$$\frac{M_\infty}{Cd}\frac{\partial Cd}{\partial M_\infty} = \frac{Cd_0}{Cd}\left(\left(\frac{M_\infty}{Cd_0}\frac{\partial Cd_w}{\partial M_\infty}\right) - b - \left(4 + \left(\frac{k_1}{K}\right)b\right)\left(\frac{KC_L^2}{Cd_0}\right)\right) \tag{A-13}$$

and

$$\frac{C_L}{Cd}\frac{\partial Cd}{\partial C_L} = \frac{Cd_0}{Cd}\left(\left(\frac{C_L}{Cd_0}\frac{\partial Cd_w}{\partial C_L}\right) + b(1+\Gamma) + \left(2 + \left(\frac{k_1}{K}\right)b(1+\Gamma)\right)\left(\frac{KC_L^2}{Cd_0}\right)\right). \tag{A-14}$$

Therefore, at the design optimum, Equations (13), (14), (15), (A-13) and (A-14) combine to give

$$\left(\frac{M_\infty}{Cd_0}\frac{\partial Cd_w}{\partial M_\infty}\right)_{DO} = \left(2 + \eta_2 + \left(\frac{k_1}{K}\right)b\right)\left(\frac{KC_L^2}{Cd_0}\right)_{DO} - (2-\eta_2)\left(\frac{Cd_w}{Cd_0}\right)_{DO} - (2{-}\eta_2 - b) \tag{A-15}$$

and

$$\left(\frac{C_L}{Cd_0}\frac{\partial Cd_w}{\partial C_L}\right)_{DO} = (1 - b(1+\Gamma_{DO})) + \left(\frac{Cd_w}{Cd_0}\right)_{DO} - \left(1 + \left(\frac{k_1}{K}\right)b(1+\Gamma_{DO})\right)\left(\frac{KC_L^2}{Cd_0}\right)_{DO}. \tag{A-16}$$

In addition, rearranging Equation (A-16) and neglecting quantities that are small compared to unity gives

$$(C_L)_{DO} \approx \left(1 - \frac{1}{2}\left(b\left(1 + \left(\frac{k_1}{K}\right)\right)(1+\Gamma_{DO}) + \left(\frac{Cd_w}{Cd_0}\right)_{DO}\left(\left(\frac{C_L}{Cd_w}\frac{\partial Cd_w}{\partial C_L}\right)_{DO} - 1\right)\right)\right)\left(\frac{Cd_0}{K}\right)_{DO}^{1/2} \tag{A-17}$$

and, using Equation (15),

$$(Cd)_{DO} \approx 2\left(1 - \frac{1}{2}\left(b\left(1 + \left(\frac{k_1}{K}\right)\right)(1+\Gamma_{DO}) + \left(\frac{Cd_w}{Cd_0}\right)_{DO}\left(\left(\frac{C_L}{Cd_w}\frac{\partial Cd_w}{\partial C_L}\right)_{DO} - 2\right)\right)\right)(Cd_0)_{DO}. \tag{A-18}$$

Hence,

$$\left(\frac{L}{D}\right)_{DO} \approx \frac{1}{2}\left(1 - \frac{1}{2}\left(\frac{Cd_w}{Cd_0}\right)_{DO}\right)\left(\frac{1}{KCd_0}\right)_{DO}^{1/2}. \tag{A-19}$$

https://doi.org/10.1017/aer.2024.10 Published online by Cambridge University Press

Appendix B. An approximate solution for the wave drag at the design optimum condition.

For simplicity, let

$$\left(\frac{Cd_w}{Cd_0}\right)_{DO} = z \text{ and } \left(\frac{C_L}{Cd_w}\frac{\partial Cd_w}{\partial C_L}\right)_{DO} = \gamma. \tag{B-1}$$

Noting that, since (k_1/K) is of order 0.1 and b is equal to 0.14, their product is of order 0.01, which is small compared to unity, Equations (A-15) and (A-16) can be written as

$$\left(\frac{M_\infty}{Cd_0}\frac{\partial Cd_w}{\partial M_\infty}\right)_{DO} \approx (2+\eta_2)\left(\frac{KC_L^2}{Cd_0}\right)_{DO} - (2-\eta_2)\,z - (2-\eta_2-b) \tag{B-2}$$

and

$$\left(\frac{C_L}{Cd_0}\frac{\partial Cd_w}{\partial C_L}\right)_{DO} = \gamma z \approx (1-b(1+\Gamma_{DO})) + z - \left(\frac{KC_L^2}{Cd_0}\right)_{DO}. \tag{B-3}$$

Hence,

$$\left(\frac{M_\infty}{Cd_0}\frac{\partial Cd_w}{\partial M_\infty}\right)_{DO} \approx (2\eta_2 - b((1+\Gamma_{DO})\,(2+\eta_2)-1)) - (\gamma\,(2+\eta_2)-2\eta_2)\,z. \tag{B-4}$$

Using Equation (39),

$$(2\eta_2 - b((1+\Gamma_{DO})\,(2+\eta_2)-1)) - (\gamma\,(2+\eta_2)-2\eta_2)\,z = 2z\,(1-\delta_{DO})\left(\frac{X}{X-j_2}\right)_{DO} \tag{B-5}$$

and, using equation (40),

$$z\left((2+\delta_{DO}\eta_2)\left(\frac{X}{X-j_2}\right)_{DO} - 2\eta_2\right) = 2\eta_2 l, \tag{B-6}$$

where

$$l = 1 - \frac{b}{2\eta_2}\left((1+\Gamma_{DO})\,(2+\eta_2)-1\right). \tag{B-7}$$

Rearranging Equation (B-6), using Equation (38) and setting

$$\left(\frac{l\eta_2 Cd_0}{j_1 (j_2)^2 cos^3(\Lambda_w)}\right) = \alpha, \tag{B-8}$$

gives

$$X_{DO}^2\,(2-(2-\delta_{DO})\,\eta_2) - X_{DO}(2-(4-\delta_{DO})\,\eta_2)\,j_2 - 2b^2\,(\eta_2+\alpha) = 0. \tag{B-9}$$

The exact solution is given by the positive value of

$$\frac{X_{DO}}{j_2} = \frac{(2-(4-\delta_{DO})\,\eta_2)}{2\,(2-(2-\delta_{DO})\,\eta_2)}\,(1 \pm f_1), \tag{B-10}$$

where

$$f_1 = \left(1 + \frac{8(2-(2-\delta_{DO})\,\eta_2)}{(2-(4-\delta_{DO})\,\eta_2)^2}\,(\eta_2+\alpha)\right)^{1/2}. \tag{B-11}$$

Hence,

$$z = j_1 (X_{DO}-j_2)^2\left(\frac{cos^3(\Lambda_w)}{(Cd_0)_{DO}}\right) = \left(\frac{cos^3(\Lambda_w)\,j_1 (j_2)^2}{4(Cd_0)_{DO}(2-(2-\delta_{DO})\,\eta_2)^2}\right) f_2, \tag{B-12}$$

where

$$f_2 = ((2-(4-\delta_{DO})\,\eta_2)\,f_1 - (2+\delta_{DO}\eta_2)^2. \tag{B-13}$$

https://doi.org/10.1017/aer.2024.10 Published online by Cambridge University Press

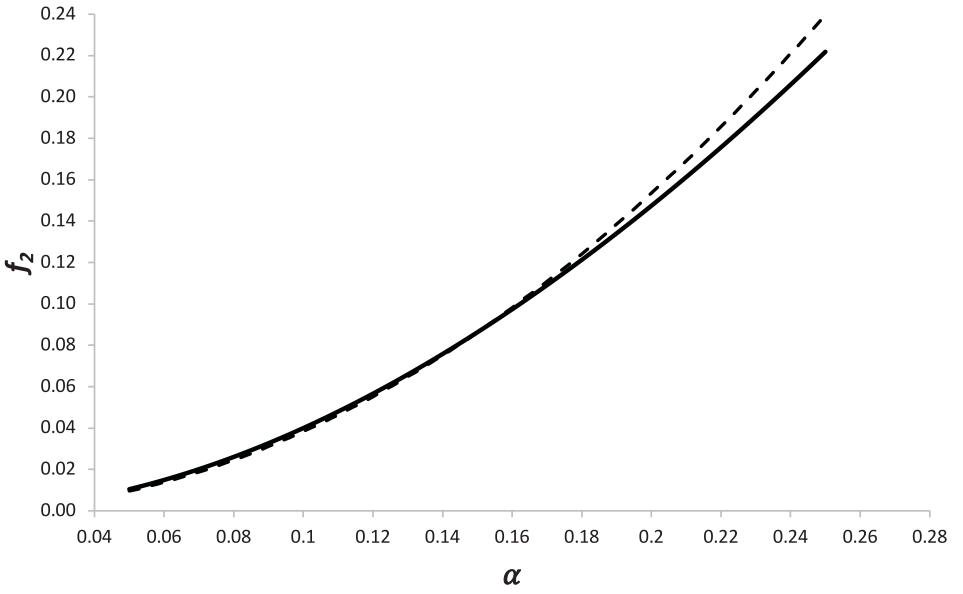

Figure B-1. *The variation of the function f_2 with α when η_2 is 0.50 and δ_{DO} is 0.2. The solid line is the exact result and the dashed line is the parabolic approximation.*

Based upon the earlier work of Poll and Schumann [4, 5], the expected parameter ranges for the current global aircraft fleet are

$$0.015 < \frac{(Cd_0)_{DO}}{cos^3(\Lambda_w)} < 0.030 \tag{B-14}$$

and

$$0.30 < \eta_2 < 0.65. \tag{B-15}$$

In addition,

$$0.6 < \frac{(C_L)_{DO}}{cos^2(\Lambda_w)} < 0.75 \tag{B-16}$$

and, hence, from Equations (34) and (41),

$$0.15 < \delta_{DO} < 0.25. \tag{B-17}$$

Therefore, in practice, the range of values for f_2 and α are bounded and, as shown in Fig. B-1, when f_2 is plotted as a function of for constant values of η_2 and δ_{DO}, the variation in the range of interest is almost parabolic, i.e.

$$f_2 \approx (F\alpha)^2. \tag{B-18}$$

where F is a constant whose value depends only upon η_2 and δ_{DO}. The values of F were chosen to give the best fit over the mid-range with equal deviations at the extremes, with the maximum deviation from the exact solution being about $\pm 10\%$. Using equation (B-7), it follows that follows that

$$\begin{aligned} z &\approx \left(\frac{\eta_2 lF}{2\,(2-(2-\delta_{DO})\,\eta_2)}\right)^2 \left(\frac{(Cd_0)_o}{j_1(j_2)^2 cos^3(\Lambda_w)}\right) \\ &\approx f_3 \left(\frac{2\eta_2+b}{2\eta_2}\right)^2 \left(1-\left(\frac{2+\eta_2}{2\eta_2+b}\right) b(1+\Gamma_{DO})\right)^2 \left(\frac{(Cd_0)_o}{j_1(j_2)^2 cos^3(\Lambda_w)}\right), \end{aligned} \tag{B-19}$$

https://doi.org/10.1017/aer.2024.10 Published online by Cambridge University Press

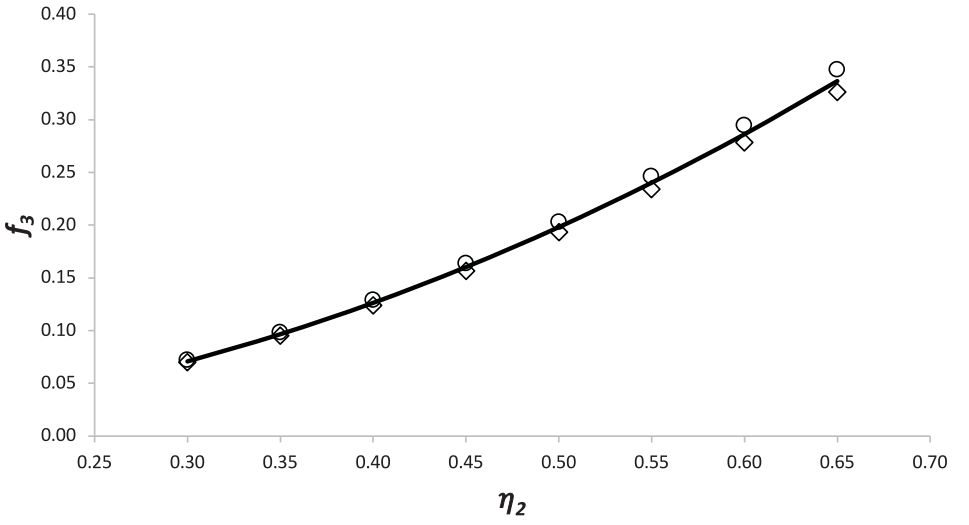

Figure B-2. *The variation of the function f_3 with η_2 and δ_{DO}. The solid line is the result for δ_{DO} equal to 0.2, the open circles are for δ_{DO} of 0.15 and the open diamonds are for δ_{DO} of 0.25.*

where

$$f_3 \approx \left(\frac{\eta_2 F}{2\,(2-(2-\delta_{DO})\,\eta_2)} \right)^2 . \tag{B-20}$$

The variation over the full parameter range is shown in Fig. B-2, where the effect of δ_{DO} is clearly very small and may be neglected.

A "least-squares" fit to get the best value of f_3 over the full variable range yields

$$f_3 \approx 0.795(\eta_2)^2 . \tag{B-21}$$

The error introduced by neglecting δ_{DO} is less than $\pm$ 3%. Since this result is insensitive to δ_{DO} it is also insensitive to uncertainties in the values of the coefficients in Equation (50).

Finally,

$$\left(\frac{Cd_w}{Cd_0} \right)_{DO} \approx \left(\frac{\sigma^2}{j_1 (j_2)^2} \right) \left(\frac{(Cd_0)_{DO}}{cos^3(\Lambda_w)} \right), \tag{B-22}$$

where

$$\sigma \approx 0.445\,(2\eta_2 + b) \left(1 - \left(\frac{2+\eta_2}{2\eta_2 + b} \right) b(1+\Gamma_{DO}) \right). \tag{B-23}$$

Appendix C. The approximate variation of the low-speed Oswald efficiency factor with the drag coefficient.

The low-speed value of the Oswald efficiency factor is given by Equations (20), (21) and (22). However, to simplify the mathematical manipulations, an approximate power law form is required, i.e.

$$e_{LS} \approx \frac{E}{(C_F^{ac})^{\tau}} \text{ where } \tau = -\left(\frac{C_F^{ac}}{e_{LS}} \right) \frac{de_{LS}}{dC_F^{ac}}. \tag{C-1}$$

From Equation (20),

$$\frac{de_{LS}}{dk_1} = -\,(\pi\,AR)\,e_{LS}^2 \tag{C-2}$$

https://doi.org/10.1017/aer.2024.10 Published online by Cambridge University Press

and, from Equation (22),

$$\frac{dk_1}{dC_F^{ac}} = \frac{k_1}{C_F^{ac}}. \tag{C-3}$$

Hence,

$$\tau = -\left(\frac{C_F^{ac}}{e_{LS}}\right)\left(-\left(\pi.AR\right)e_{LS}^2\right)\frac{k_1}{C_F^{ac}} = \pi.AR.k_1.e_{LS}, \tag{C-4}$$

and

$$E = e_{LS}\left(C_F^{ac}\right)^{\tau}. \tag{C-5}$$

Appendix D. Relations linking static pressure, indicated altitude and flight level.

As described in Poll [3] and Poll and Schumann [4], "altitude" is determined by comparing ambient static pressure, p_∞ with a reference pressure, p_{ref}, specified by Air Traffic Management (*ATM*). The altimeter then provides an indicated altitude (*IA*) by using the variation of height versus p_∞/p_{ref} in the International Standard Atmosphere [6]. For take-off and landing, p_{ref} is the local airport pressure (the *QFE*) and so *IA* is measured relative to the runway. At an *ATM* specified height above the airport, p_{ref} is set to the actual pressure at sea level (the *QNH* or "regional" pressure) and, consequently, the *IA* is measured relative to sea level. Finally, as the aircraft passes through the *ATM* determined "transition" altitude, p_{ref} is set to the *ISA* sea level pressure (1.01325 bars) and the *IA* is the height above sea level that the aircraft would have in the *ISA*. Since the vertical variation of ambient pressure and temperature on any particular day is unlikely to be the same as in the *ISA*, the indicated altitude will probably not be the true geometric value. To avoid any ambiguity, above the transition altitude, the term flight level (*FL*) is used. Therefore, an aircraft flying at a fixed flight level is following an isobar. Flight level is defined as the indicated altitude divided by 100. Hence, if the ambient pressure is given in bars, when p_∞ is greater than 0.2263204 bars, the flight level is

$$FL = \frac{IA\ (feet)}{100} = 1454.422\left(1 - 0.9974987p_\infty^{0.190263}\right), \tag{D-1}$$

otherwise

$$FL = \frac{IA\ (feet)}{100} = 51.75864\left(1 - 4.019779ln(p_\infty)\right). \tag{D-2}$$

Appendix E. An estimate of the effect of reducing Cd_0 on the optimum cruise flight level.

Differentiating Equations (50) and (51) gives

$$\frac{d(C_L)_{DO}}{(C_L)_{DO}} = \frac{1}{2}\frac{d(Cd_0)_{DO}}{(Cd_0)_{DO}} \text{ and } \frac{d(L/D)_{DO}}{(L/D)_{DO}} = -\frac{1}{2}\left(\frac{d(Cd_0)_{DO}}{(Cd_0)_{DO}}\right). \tag{E-1}$$

From Equation (3), the total fuel required for the flight, usually called the trip fuel, $(m_f)_{trip}$, is almost inversely proportional to *L*/*D* and so

$$\frac{d\left(m_f\right)_{trip}}{\left(m_f\right)_{trip}} \approx -\frac{d(L/D)_{DO}}{(L/D)_{DO}}. \tag{E-2}$$

Hence, since the take-off aircraft mass, *MTO*, is the sum of the trip fuel mass and a constant mass comprising the structure weight, the payload and the reserve fuel,

$$\frac{dMTO}{MTO} \approx -\left(\frac{\left(m_f\right)_{trip}}{MTO}\right)\frac{d(L/D)_{DO}}{(L/D)_{DO}} = \frac{1}{2}\left(\frac{\left(m_f\right)_{trip}}{MTO}\right)\left(\frac{d(Cd_0)_{DO}}{(Cd_0)_{DO}}\right). \tag{E-3}$$

https://doi.org/10.1017/aer.2024.10 Published online by Cambridge University Press

Near the tropopause, the variation of flight level with ambient pressure is given approximately by Equation (91). Therefore, if $(C_L)_{DO}$ changes due to a change in Cd_0,

$$\frac{d(FL)_{DO}}{(FL)_O} \approx \frac{0.61}{2} \left(\frac{d(Cd_0)_{DO}}{(Cd_0)_{DO}} \right) \tag{E-4}$$

and, if $(m_f)_{trip}$ changes due to a change in Cd_0,

$$\frac{d(FL)_{DO}}{(FL)_{DO}} \approx -\frac{0.61}{2} \left(\frac{(m_f)_{trip}}{MTO} \right) \left(\frac{d(Cd_0)_{DO}}{(Cd_0)_{DO}} \right). \tag{E-5}$$

Consequently, the total change in flight level resulting from a change in Cd_0 is

$$\frac{d(FL)_{DO}}{(FL)_{DO}} \approx \frac{0.61}{2} \left(1 - \left(\frac{(m_f)_{trip}}{MTO} \right) \right) \left(\frac{d(Cd_0)_{DO}}{(Cd_0)_{DO}} \right). \tag{E-6}$$

Since the ratio of trip fuel mass to take-off mass can never exceed unity, all other things being equal, a decrease in Cd_0 always lowers the optimum cruise flight level.

Cite this article: Poll D.I.A. and Schumann U. (2024). On the conditions for absolute minimum fuel burn for turbofan powered, civil transport aircraft and a simple model for wave drag. *The Aeronautical Journal*, **128**, 1071–1103. https://doi.org/10.1017/aer.2024.10

https://doi.org/10.1017/aer.2024.10 Published online by Cambridge University Press

https://dspace.org/

On the conditions for absolute minimum fuel burn for turbofan powered, civil transport aircraft and a simple model for wave drag

Poll, D. I. A.; Schumann, Ulrich

2024-06-01
Cambridge University Press (CUP)
https://doi.org/10.1017/aer.2024.10
Poll DIA, Schumann U. (2024) On the conditions for absolute minimum fuel burn for turbofan powered, civil transport aircraft and a simple model for wave drag. The Aeronautical Journal, Volume 128, Issue 1324, June 2024, pp. 1071-1103

Downloaded from a DSpace repository. https://dspace.org/